Hindawi
Journal of Sensors
Volume 2022, Article ID 8921779, 23 pages
https://doi.org/10.1155/2022/8921779

Research Article

Nonlinear Dynamic Analysis of Hybrid Piezoelectric-Magnetostrictive Energy-Harvesting Systems

K. Niazi, M. J. Kazemzadeh Parsi, and M. Mohammadi

Department of Mechanical Engineering, Shiraz Branch, Islamic Azad University, Shiraz, Iran

Correspondence should be addressed to M. J. Kazemzadeh Parsi; kazemzadeh@iaushiraz.ac.ir

Received 13 May 2022; Revised 14 July 2022; Accepted 20 July 2022; Published 5 August 2022

Academic Editor: Mohamed Louzazni

To progress the proficiency and broaden the action bandwidth of vibration energy harvesters, this paper presents a cantilever piezoelectric-magnetostrictive bistable hybrid energy harvester with a dynamic magnifier. The hybrid energy-harvesting system comprises two vibration degrees of freedom and two electrical degrees of freedom. It consists of a composite cantilever beam made of three layers, in which the magnetostrictive and piezoelectric layers are attached to the top and bottom of the base layer. The electromechanically coupled vibration equations of the whole hybrid structure were established with the lumped-parameter model while taking into account the magnetic interaction of two magnets. The nonlinear frequency-response of vibrations for the hybrid harvester is calculated using the harmonic balance method, and the model has been validated by literature. The time response and phase portraits of oscillation for the cantilever harvester and its performance in generating electrical power under different magnet distances, dynamic magnifier features, and excitation levels are analyzed. Numerical results have shown that the hybrid structure can harvest additional electrical power and operates at larger bandwidth than routine bistable piezoelectric or magnetostrictive energy harvesters.

1. Introduction

With a quickly increasing market for solid-state electronics, energy consumption demanded by microelectronic tools has been reduced, which helps the progress of energy-harvesting technology. Between lots of energy sources, energy harvesting from mechanical vibration has developed wide-ranging because of availability [1], besides harvesting from the ambient vibrations is much considered. In the past years, many scholars have considered vibration energy-harvesting (VEH) systems which are electromagnetic-, electrostatic-, and piezoelectric-based devices. Besides, there is a new type, magnetostrictive harvesting, which developed in recent years [2].

To broadband operating frequencies of VEH systems, researchers have established some resolutions such as tuning techniques, multimodel systems, and nonlinear systems [3]. Scientists have used nonlinear methods to make energy harvesting available in a broadband frequency extensively. The bistable structure was formed by the nonlinear magnetic force between repulsive magnets, and the magnification mechanism is presented to increase the base excitation. The bistable energy harvesting (BEH) can produce a large-amplitude motion with high power by means of broadening the bandwidth greatly. One of the most familiar arrangements for BEH is the magnetic repulsion harvester in which the nonlinearity governed by the repulsion force can greatly increase the harvesting power [4]. In recent years, the nonlinear bistable energy-harvesting (BEH) systems have received extensive attention, since they act over a further wide range of base excitation frequencies and can lead to extra output power [5].

Erturk et al. [6] showed that the piezoelectric BEH excited by harmonic inputs can show large-amplitude periodic or chaotic motions. Ferrari et al. [7] compared the displacement response of a BPEH under band-limited excitation and confirmed the results by tests. Karami and Inman [8] considered the perturbation method for BPEH in the initial resonance state. Kim and Seok [9] planned multistable PBEH to extract power in broadband frequencies, even at low excitation levels. Pan and Dai [10] considered composite laminate with a new stacking sequence to regulate

the resonance frequency of the PBEH and improved the vibration behaviors of the harvester. The lumped-parameter model with magnetic coupling has been considered for broadening the resonance frequency range of nonlinear bistable vibration energy harvester by Jiang et al. [11]. Nguyen et al. [12] developed the magnetically coupled 2-DOF bistable vibration energy harvester with a high-energy trajectory, increasing the resonance frequency and elevated electrical power. The nonlinear magnetic force has been used to establish the electromagnetic bistable vibration system by Wang et al. [13] to improve its effectiveness in broadening the resonance bandwidth of the harvester. Kianpoor and Jahani [14] considered the output power which is from rectangular and trapezoidal bimorph piezoelectric cantilever beams with tip mass analytically and optimized the harvester geometry by implementing the genetic algorithm. Time and frequency-response analyses of functionally graded piezoelectric CNT-reinforced cantilever harvesters have been studied by Heshmati and Amini [15] for harmonic and random excitations using finite element formulation. Wu and Xu [16] studied a bistable piezoelectric energy harvester compounds' elastic and gravitational potential energy.

There are some arrangements of elastic magnifiers that are generally displayed as a linear mass-spring system positioned between the bimorph beam and the base. Aladwani et al. [17] analyzed a PEH containing a simple spring magnifier using finite element theory. Vasic and Costa [18] developed a double beam harvester with a magnifier to investigate the added harvesting power of a traditional harvester. Dynamic analysis of bistable PEH with elastic magnifier configuration has been considered by Wang and Liao [19] based on lumped-parameter model and then verified experimentally. Wang et al. [20] use an arrangement with an auxiliary mass-spring magnifier to strengthen base excitation and deliver appropriate dynamic energy to overcome potential wells, hence leading to large-amplitude bistable motion. Bernard and Mann [21] merged the features of the dynamic amplifier and nonlinear modified energy-harvesting system to enhance the total harvesting bandwidth and improve the harvested power.

Vibration energy harvesting based on magnetostrictive (Ms) materials (MsM), which are a recent category of a smart material, uses the change of magnetic flux density by cause of the structural vibrations and produces voltage all over a pick-up coil. MsM such as galfenol (iron-gallium alloy) and Metglas (glass fiber metal compound) have increasingly developed, in recent years. Because of their physical features, for example, high-energy density, it seems galfenol-based harvesters are able to deliver better energy generating and performance. In comparison with the piezoelectric harvester, the magnetostrictive power harvester does not entail high corresponding impedance and evades the leakage problems and depolarization. Thus, the attention of researchers has been attracted by magnetostrictive vibration harvesters in this decade [22].

Ueno and Yamada [23] established a bimorph energy harvester based on two cantilever beams of galfenol. Magnetostrictive vibration energy harvester made of Fe-Ga alloy was studied by Kita et al. [24]; 35% of conversion efficiency was reached at an input frequency of 202 Hz. Damping and energy harvesting of the magnetostrictive vibrations system have been discussed in Fang et al. [25]. Based on thermodynamic free-energy density approach and finite element model, Ahmed et al. [26] proposed a magnetostrictive vibration energy harvester concerning the steady-state response of the oscillation. Cao et al. [27] established the 2-DOF nonlinear magneto-electro-mechanic coupled model of a galfenol nonlinear cantilever energy harvester + dynamic magnifier (DM), analytically. They illustrated the influence of some key parameters such as mass and stiffness ratios on output voltage and power. Zhang et al. [28] analyzed a NES–magnetostrictive coupled model based on cantilever beam for vibration control and energy harvesting using the harmonic balance method by means of COMSOL Multiphysics. Clemente et al. [29] examined the behavior of an energy harvester device exploits three rods of galfenol. Liu et al. [30] selected a magnetostrictive material for the vibration harvesting system and studied a magnetostrictive bistable vibration harvester with displacement magnification instrument.

To overcome the energy-incompetency concern of a single-energy harvester, hybrid energy-harvesting technology has been developed. This fusion harvester can be divided into two groups: multisource hybrid harvesters and single-source harvesters with combination mechanisms. The second one characterizes converting energy into electricity through various forms of transduction structures, where hybrid materials, structures, and devices are proficient in developing energy conversion efficiency. Wang et al. [31] investigated a 2-DOF hybrid piezoelectric-electromagnetic energy harvester to enhance the harvested power from the electromechanical transducer. Stochastic dynamics of the hybrid energy harvester were considered by Sengha et al. [32] concerning the nonlinear magnetic coupling. Considering the piezomagneto-elastic energy-harvesting system under low-frequency excitations, Jahanshahi et al. [33] studied the application of secondary resonances in multifrequency excitations. Fang et al. [34] proposed a bistable rotational energy-harvesting system with hybrid piezoelectric and electromagnetic mechanisms for increasing harvested power at the low-frequency excitation. Modeling and theoretical study of a piezoelectric-electromagnetic hybrid energy harvesting from vortex shedding-induced vibration have been considered by Li et al. [35]. This study deals with a hybrid piezoelectric-magnetostrictive energy harvester carrying the magnet at the free end while a magnifier connected them to the base. The hybrid vibration energy harvester includes both piezoelectric-based and magnetostrictive-based energy harvester systems. The harvester consists of a three-layered cantilever beam with a core and smart faces while taking into account the magnetic interaction of two magnets. To quantify the responses, a lumped-parameter model of the simulation system is established.

2. Structure design of Novel hybrid vibration Energy Harvester (HVEH)

The structure of the hybrid magnetostrictive-piezoelectric (Ms-P) vibration harvesting system with a dynamic magnifier (DM) is developed in this study and shown in Figure 1.

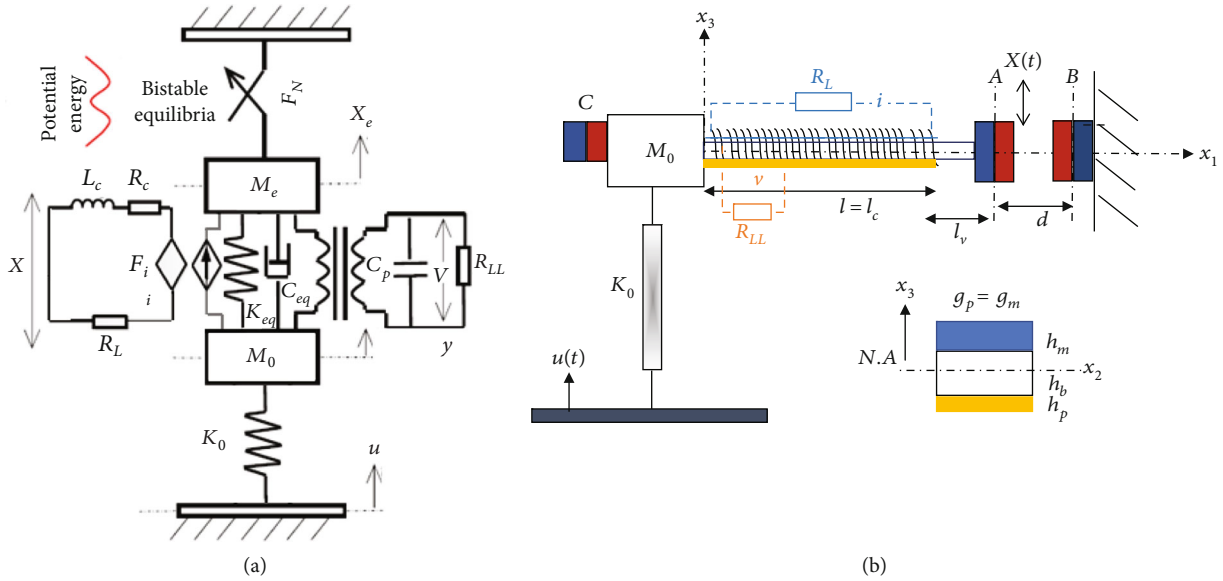

FIGURE 1: (a) 2-DOF nonlinear lumped-parameter model of the hybrid energy harvester (HEH) + DM. (b) Schematic structure of piezoelectric-magnetostrictive harvesting system with DM.

The bistable hybrid power generation system uses both piezoelectric and Ms layers to convert vibrational energy into electrical energy. It consists of a composite cantilever beam made of three layers, in which the magnetostrictive and piezoelectric layers are attached to the top and bottom of a metalic core through the epoxy adhesive glue, respectively. The surface of the piezoelectric layer is completely enclosed with a tinny electrode, and a resistance R_{LL} is coupled to the piezoelectric energy harvester electrically. Also, a pick-up coil, with resistance R_c, turns N, length $l_c \approx l_m$, and cross-sectional area $S_c \approx g_m h_m$, is bounded on the cantilever and linked in series with resistance R_L; the power collection part is simplified as the load impedance.

As shown in Figure 1 magnet A is attached to the beam free end; its magnetic field direction is a reverse polarity to the field of another fixed magnet B. The two-part permanent magnets are mutually repellent and creates a bistable structure. The distance between two magnets A and B are denoted by d, measured according to the undeformed shape of the beam. By adjusting the parameter d, the force between them is varied. When this distance is proper, the system is bistable.

Two magnets A and C provide a bias magnetic field $H_b = 3580$ A/m for the Ms layer. Magnets A, B, and C have the same volume, $V_A = V_B = V_C$, and their magnetizations are M_A, M_C, and M_B. The beam's longitudinal axis is x_1, whereas the transverse axis is x_3, so that the $x_1 - x_3$ plane is set on the neutral plane of the beam. The DM consists of a mass and a spring element which is positioned between the BHEH and the base. The whole vibration harvesting system is simplified as a 2-DOF lumped-parameter nonlinear vibration model, when the cantilever beam vibrates in the first-order mode, as shown in Figure 1, in which M_0 and K_0 denote the equivalent mass and stiffness of the DM, respectively; l is the total effective length of the beam $(l = l_b + l_v)$, in which $l_v = 20mm$; Furthermore h_p, h_m, and h_b are the thickness of the piezoelectric, Ms, and core layers, respectively.

Besides, M_e, K_e, C_e, and ω_e are the equivalent (effective) mass, stiffness, damping, and resonant frequency of the cantilever beam, respectively, where $M_e = M_t + (33/140)m$, $K_e = 3EI_b/l^3$ [36]. In which M_t is the tip mass and equals to $M_t = \rho_A \times V_A$ (the product of the density and the volume of the magnet A). Also m, E, and ζ are the composite beam's mass, Young's modulus, and damping ratio, respectively. EI_b is the average stiffness of the beam, and I_b is the moment of inertia of the beam cross-section about the neutral axis. An acceleration $\ddot{u}$ is applied to the base, and the displacement of the mass M_e and M_0 are written as $x_e(t)$ and $y(t)$, respectively. Using relative motion x, $(x = x_e - y)$.

The system currently has two steady-state equilibria, and the harvester displays bistable features. In this arrangement, the force among magnets A and B is regulated by changing the distance d. Also, the mass ratio $(r_m = M_0/M_e)$ and stiffness ratio $(r_k = K_0/K_e)$ of the DM could change the vibration behavior of the 2-DOF harvester.

3. Theoretical Model of Harvesting System

3.1. Magnetostrictive Layer Subsystem (Modeling of the Magnetostrictive Part). When the harvester vibrates, because of the Villari effect, the magnetic induction B_z in MsM (Galfenol) is varied, so the current i and magnetic field H_c in the coil are induced, in which $H_c = Ni/l_c$ $(N = 1000\ turns)$. The constitutive equations for Ms layer are [37]:

$$\varepsilon_M = \frac{\sigma_M}{E_M} + d_M H_z, \tag{1}$$

$$B_z = d_M \sigma_M + \mu H_z, \tag{2}$$

where ε_M denotes the strain, $H_z = H_b + H_c$ signifies the strength of magnetic field, σ_M is the stress applied to the MsM, and E_m is the Young's modulus of the MsM; $d_M = 34\,\mathrm{T/GPa}$ is piezomagnetic coefficient, and μ is magnetic permeability which $\mu = 230\,\mu_0$ is taken in this paper. The strain is $\varepsilon = 3\tilde{h}(0.65l - l)x/l^3$ [37] where $\tilde{h}$ is the distance from the neutral axis of beam cross-section to the center of Ms layer. x is the relative displacement of the beam tip, and l is the beam effective length as mentioned before. When $\varepsilon_M = 0$, Equation (1) becomes $\sigma_M = -E_M d_M N i/l_c$, and the average stress σ_M^i associated with i is given as [37]:

$$\sigma_M^i = \frac{1}{(h_m + h_c + h_p) l_m} \int_0^{l_m} \int_0^h \frac{F_i}{I_b} (l - x_1) x_3 dx_3 dx_1 = \frac{F_i (2l - l_m)\tilde{h}}{4I_b}. \tag{3}$$

The force F_i derivative by Equation (3) is:

$$\begin{aligned} F_i &= -d_M k_i i, \\ k_i &= \frac{4E_M I_b N}{\tilde{h}(2l - l_m) l_c}, \end{aligned} \tag{4}$$

From Equations (1) and (3), the magnetic field strength B_z can be found as:

$$B_z = \frac{3d_M E_M \tilde{h}(0.65l - l)x}{l^3} + \left(\mu - E_M {d_M}^2\right)(H_b + Ni/l_c). \tag{5}$$

Considering the electrical part of the Ms layer subsystem, the induced voltage v_M in the pick-up coil with length l_c using faraday law is [38]:

$$\frac{dv_M}{dx_1} = \frac{-NS_c}{l_c} \frac{dB_z}{dt}. \tag{6}$$

Replacing Equation (5) into Equation (6) and participating in the subsequent equation with respect to x_1 yields, the harvested voltage of the MsM harvester part is:

$$v_M = \beta \frac{dw}{dt} - L_c \frac{di}{dt}. \tag{7}$$

in which [37]:

$$\begin{aligned} \beta &= \frac{3d_M N S_c E_M \tilde{h}(2l - l_m)}{2l^3}, \\ L_c &= \left(\mu - E_M {d_M}^2\right)\left(N^2 S_c / l_c\right). \end{aligned} \tag{8}$$

Now, the output voltage of the Ms harvester is expressed as $v_M = (R_L + R_C)i$, considering the coil resistance R_C and load resistance R_L, so the electrical equation of the subsystem is expressed as:

$$\beta \frac{dw}{dt} - L_c \frac{di}{dt} - Ri = 0. \tag{9}$$

3.2. Piezoelectric Layer Subsystem. For the piezoelectric layer attached to the cantilever beam, the piezoelectric constitutive equation can be written as [36]:

$$\varepsilon_p = c_{11}^{-1} \sigma_p + d_{31} E_z, \tag{10}$$

$$D_z = d_{31} \sigma_p + \varepsilon_{33}^T E_z, \tag{11}$$

Where E_z and D_z characterize the electric field and displacement in the z-direction, consistently. ε_p is the strain in the x-direction; $s_{11=}\, {c_{11}}^{-1}$ is the compliance coefficient under a constant electric field; σ_p is the stress in the x-direction; d_{31} is the piezoelectric coefficient; E_z is the electric field strength in the x_3-direction; D_z is the electric displacement in the x_3-direction; ${\varepsilon^T}_{33}$ is dielectric coefficient under constant stress.

From Equation (10), under zero strain, $\sigma_p = -e_{31} v/h_p$, where $e_{31} = c_{11} d_{31}$, is the piezoelectric constant. Furthermore, $v = E_z h_p$. There is also an electromechanical coupling force F_p related to the voltage v, as follows [39]:

$$\sigma_p = \frac{1}{l_e} \int_0^{l_e} \frac{F_p (l - x_1)\left(h_p + h_b\right)}{2I} dx_1 = \frac{F_p (2l - l_e)\left(h_p + h_b\right)}{4I}, \tag{12}$$

where h_b is the thickness of the cantilever beam, l_e is the length of the piezoelectric layer, and u is the displacement from the center of the beam along the beam axis. From Equation (12), one can write:

$$F_p = -\kappa_v v\,; \kappa_v = \frac{4Ie_{31}}{h_p (2l - l_e)\left(h_p + h_b\right)}. \tag{13}$$

Consider the relationship between the mass displacement x and the generated current i when $E_z = 0$. It can be obtained from Equation (12):

$$D_z = d_{31}\sigma_p = d_{31} E_p \varepsilon_p = \frac{3e_{31}(2l - l_e)\left(h_p + h_b\right)}{4l^3} x, \tag{14}$$

where E_p is the elastic modulus of the piezoelectric layer, Then:

$$\begin{aligned} i &= 2bl_e \frac{dD_z}{dt} = \kappa_c \frac{dx}{dt}, \\ \kappa_c &= \frac{3l_e e_{31}(2l - l_e)\left(h_p + h_b\right)}{2l^3}. \end{aligned} \tag{15}$$

Considering the Piezoelectric subsystem, the electrical equation based on the Kirchhoff's law is expressed as [36]:

$$\kappa_c \frac{dX}{dt} + \frac{v}{R_p} + C_p \frac{dv}{dt} = 0. \tag{16}$$

v is the voltage across the load, C_p is the equivalent capacitance of the piezoelectric layer, and R_p is the load resistance.

4. Coupling Model and Equation of Motion

The electromechanically coupled nonlinear equations of the hybrid harvester may be found by combination of the ordinary differential equations of the Ms and piezoelectric parts as follows:

$$\begin{aligned} &M_e\frac{d^2x_e}{dt^2}+C_e\frac{dx}{dt}+K_ex-F_N-F_v-F_i=0\,;\,(x_e=x+y),\\ &M_0\frac{d^2y}{dt^2}+K_0(y-u)-\left(K_ex+C_e\frac{dx}{dt}\right)+F_v+F_i=0,\\ &\kappa_p\frac{dx}{dt}+C_p\frac{dv}{dt}+\frac{v}{R_L}=0\,;\\ &\beta\frac{dx}{dt}-L_c\frac{di}{dt}-R_ci=0, \end{aligned} \tag{17}$$

where the nonlinear vertical force F_N, based on the Taylor series, is [30]:

$$F_N=k_1(x_e-y)+k_3(x_e-y)^3. \tag{18}$$

k_1 and k_3 are the linear and nonlinear spring constants [30].

$$k_1=\frac{3\mu_0V_AV_BVM_AM_B}{2\pi ld^4}\,;k_3=k_1\left(\frac{1}{l^2}+\frac{5}{d^2}\right). \tag{19}$$

So, the coupled equations of hybrid 2-DOF piezoelectric harvester rewrite as follows:

$$\begin{aligned} &M_e\frac{d^2x}{dt^2}+C_e\frac{dx}{dt}+(K_e-k_1)x+k_3x^3-\kappa_v v+k_id_Mi+M_e\frac{d^2y}{dt^2}=0,\\ &M_0\frac{d^2y}{dt^2}+K_0y-\left(K_ex+C_e\frac{dx}{dt}\right)+\kappa_v v-k_id_Mi-K_0u=0,\\ &\kappa_p\frac{dx}{dt}+C_p\frac{dv}{dt}+\frac{v}{R_L}=0,\\ &\beta\frac{dx}{dt}-L_c\frac{di}{dt}-R_ci=0. \end{aligned} \tag{20}$$

Dimensionless equation can be obtained as:

$$X^{\cdot\cdot}[T]+2\zeta X'[T]-aX[T]+bX[T]^3-\Delta V[T]+\gamma I[T]+Y^{\cdot\cdot}[T]=0, \tag{21}$$

$$Y^{\cdot\cdot}[T]+\frac{r_k}{r_m}Y[T]-\frac{2\zeta}{r_m}X'[T]-\frac{1}{r_m}X[T]+\frac{\Delta}{r_m}V[T]-\frac{\gamma}{r_m}i[T]-\frac{r_k}{r_m}U[T]=0, \tag{22}$$

$$\kappa^2X'[T]+V'[T]+\Theta_1V[T]=0, \tag{23}$$

Table 1: Physical and material properties of the model, including piezoelectric and MsM.

Parameters	Values
Layer thickness (mm)	$h_p=0.5$, (Piezo layer) $h_m=0.75$, (Ms layer) $h_b=1.25$ (substrate)
Beam width (mm)	$g_p=g_m=g_b=8$
Beam lengths (mm)	$l_p=32$, (Piezo layer) $l_m=l_b=38$, (substrate, Ms layer)
Elastic modulus (GPa)	$E_p=66$, (Piezoelectric) $E_m=70$, (MsM) $E_b=68$ (substrate)
Density (kg/m)	$\rho_m=2700$(MsM), $\rho_b=7800$, (substrate) $\rho_p=7800$, (Piezoelectric) $\rho_A=8000$, (Tip Magnet A)
Magnet volume $\left(\text{mm}^3\right)$	$V_A=5.13\times14.14^2$; $V_B=V_A$;
Magnet intensity (A/m)	$M_A=3.2\times10^6$; $M_B=1\times10^6$; $M_C=1.8\times10^6$
Magnetic permeability (H/m)	$\mu=230\mu_0$; $\left(\mu_0=4\pi\times10^{-7}\,;\right)$
Load resistance (ohm)	$R_c=36.4\Omega\,(coil)$; $R_L=100\Omega\,(Ms\ circut)$; $R_{LL}=25k\Omega$; $(piezo\ circut)$
Dielectric permittivity (F/m)	$\epsilon_{33}=1800\,\epsilon_0$; $\left(\epsilon_0=8.854\times10^{-12}\right)$;
Piezoelectric constant (C/m)	$d_{31}=190\times10^{-12}$
Piezomagnetic coefficient (T/Pa)	$d_M=34\times10^{-9}$;

$$\Theta_2X'[T]-I'[T]-\alpha I[T]=0, \tag{24}$$

where the nondimensional parameters and coefficients are defined as:

$$\begin{aligned} &X=\frac{x}{l}\,;Y=\frac{y}{l}\,;\omega_e=\sqrt{K_e/M_e}\,;\zeta=\frac{C_e}{2\sqrt{M_eK_e}}\,;T=\omega_et,\\ &V=\frac{v}{e_v}\,;e_v=\frac{M_eg}{\kappa_v}\,;\Delta=\frac{M_eg}{K_el}\,;\kappa^2=\frac{\kappa_pl}{C_pe_v}\,;\Theta_1=\frac{1}{\omega_eR_LC_p},\\ &I=\frac{i}{e_i}\,;e_i=\frac{M_eg}{k_id_M}\,;\alpha=\frac{R_c}{\omega_eL_c}\,;\Theta_2=\frac{\beta l}{e_iL_c}\,;\gamma=\frac{k_id_M}{K_el}. \end{aligned} \tag{25}$$

Assuming $z_1(T)=X(T), z_2(T)=X'(T), z_3(T)=Y(T), z_4(T)=Y'(T), z_5(T)=V(T), z_6(T)=I(T)$, the state space form of system equations are as follows:

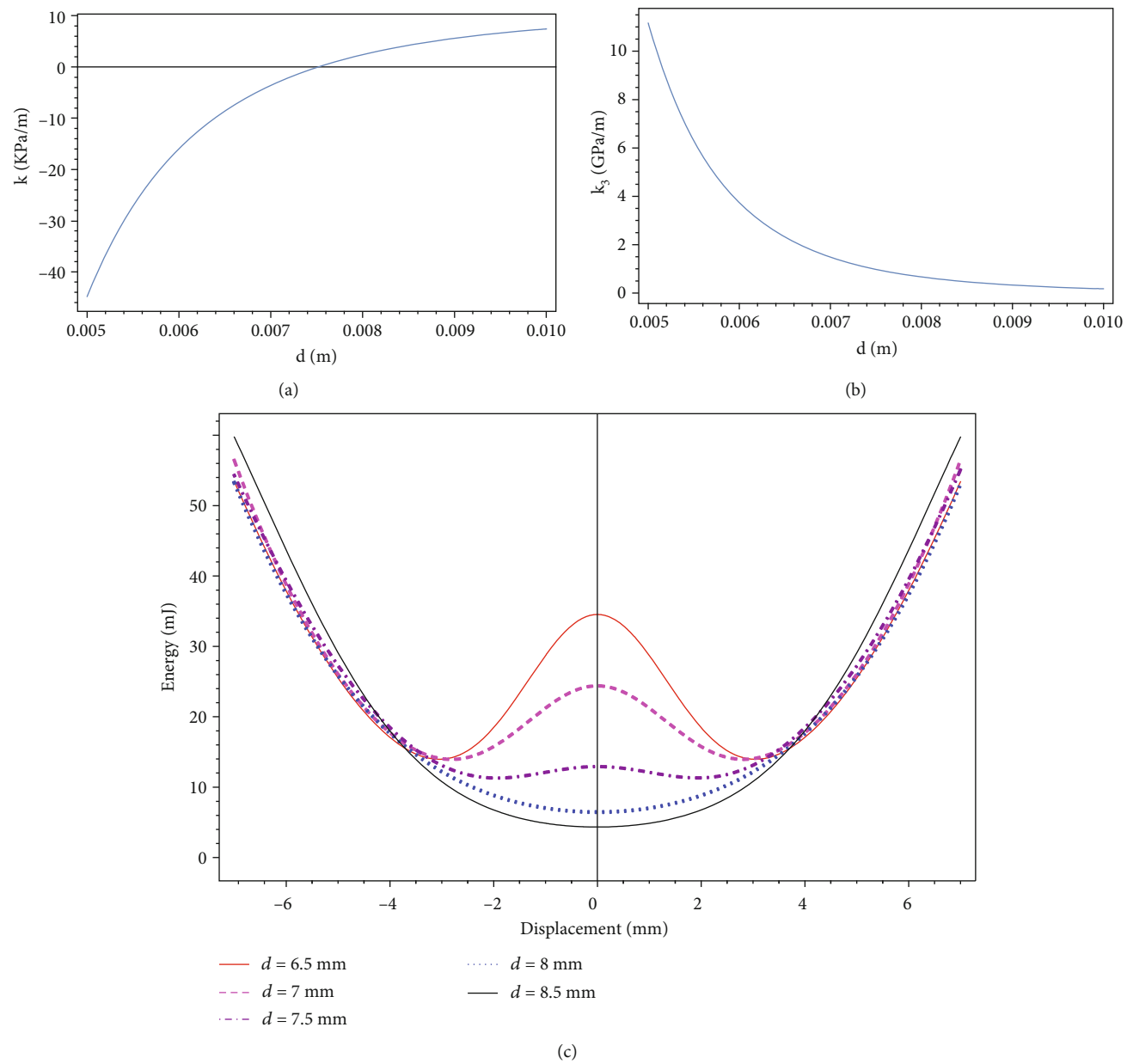

FIGURE 2: (a) Linear stiffness and (b) nonlinear stiffness curves of harvester versus d parameter. (c) Potential energy versus free end of cantilever beam displacement curve.

$$\frac{d}{dT}\begin{Bmatrix} z_1 \\ z_2 \\ z_3 \\ z_4 \\ z_5 \\ z_6 \end{Bmatrix} = \begin{Bmatrix} z_2 \\ az_1 - bz_1^3 - 2\zeta z_2 + \Delta z_5 - \gamma z_6 \\ z_4 \\ [z_1 + 2\zeta z_2 + r_k z_3 - \Delta z_5 + \gamma z_6]/r_m \\ -\kappa^2 z_2 - \Theta_1 z_5 \\ \Theta_2 z_2 - \alpha z_6 \end{Bmatrix} + \begin{Bmatrix} 0 \\ 0 \\ 0 \\ r_k/r_m \\ 0 \\ 0 \end{Bmatrix} \ddot{U}_b(T). \tag{26}$$

5. Frequency Domain Analysis of the System

In this section, the frequency domain solution of the nonlinear hybrid harvester was analyzed using the harmonic balance method. According to the dimensionless coupled equation of motions, disposing of Equation (21), one can obtain:

$$Y[T] = \gamma\left(\frac{1+r_m}{r_k}\right)I[T] - \Delta\left(\frac{1+r_m}{r_k}\right)V[T] + \left(\frac{1-ar_m}{r_k}\right)X[T] + \frac{br_m}{r_k}X[T]^3 + 2\zeta\left(\frac{1+r_m}{r_k}\right)X'[T] + \frac{r_m}{r_k}X''[T] + U[T]. \tag{27}$$

Then:

$$Y''[T] = \frac{(1+r_m)\gamma}{r_k}I''[T] - \frac{(1+r_m)\Delta}{r_k}V''[T] + \frac{(1-ar_m)}{r_k}X''[T] + \frac{3br_m}{r_k}X[T]^2X''[T] + \frac{6br_m}{r_k}X[T]X'[T]^2 + \frac{2(1+r_m)\zeta}{r_k}X^{(3)}[T] + \frac{r_m}{r_k}X^{(4)}[T] + U''[T]. \tag{28}$$

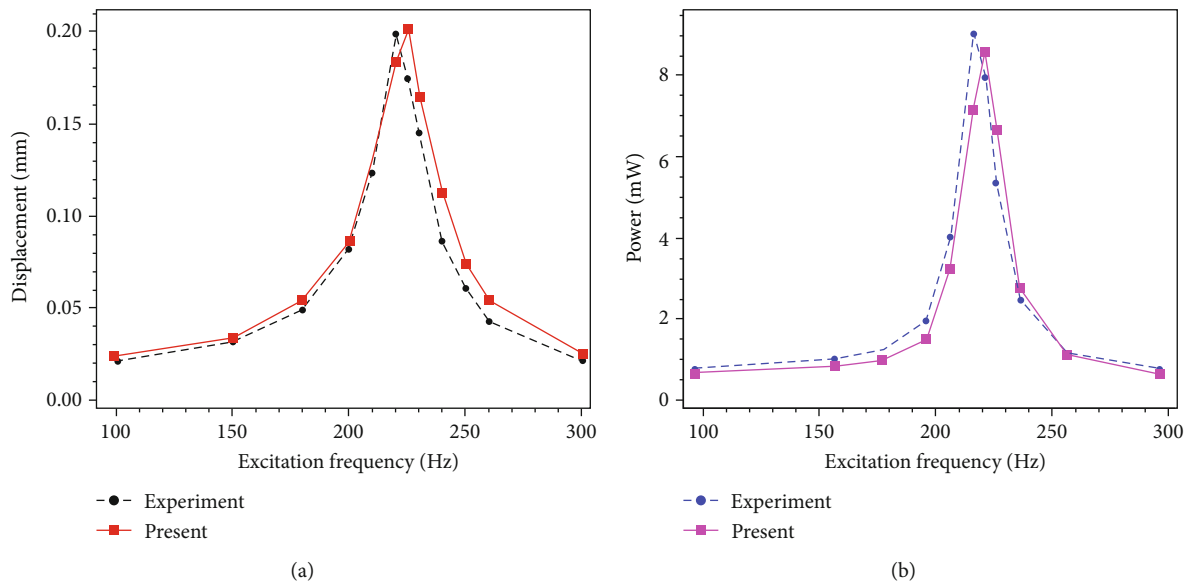

Figure 3: Comparison of obtained numerical results) with experimental results from Yoo and Flatau [40], for (a) max displacement and (b) harvested power versus excitation frequency, when $R_L = 100$.

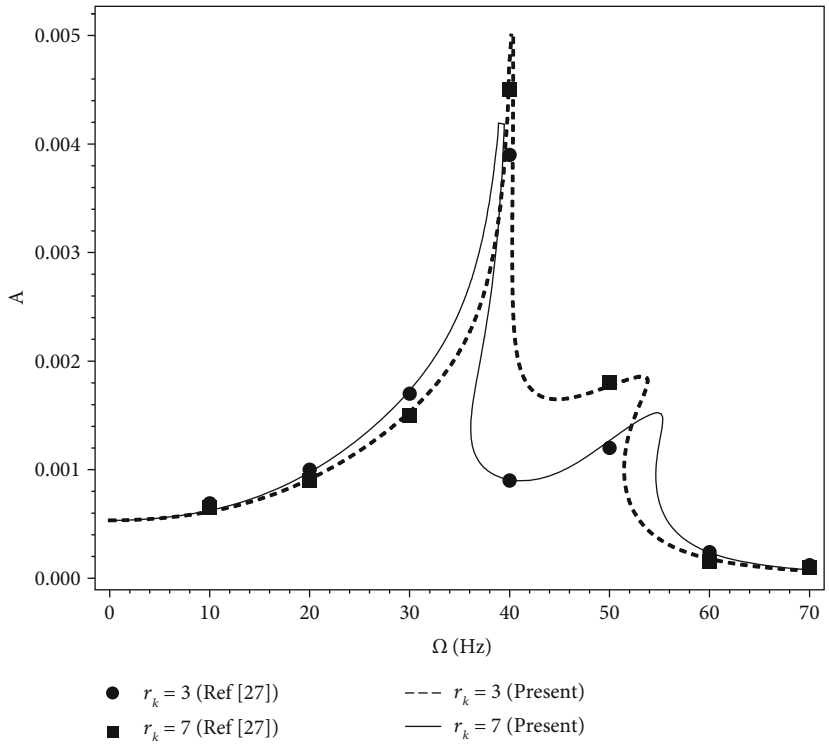

Figure 4: Verification of frequency-response result with ref. [27].

Substituting Equation (27) into Equation (21), a 4th-order nonlinear differential equation is attained as follows:

$$\frac{r_m}{r_k}X^{(4)}[T] + \frac{2\zeta(r_m+1)}{r_k}X^{(3)}[T] + \left(1 + \frac{1}{r_k} - \frac{ar_m}{r_k}\right)X''[T] + 2\zeta X'[T] - aX[T] + bX[T]^3 + \frac{br_m}{r_k}\left(6X[T]X'[T]^2 + 3X[T]^2X''[T]\right) + \gamma I[T] + \frac{\gamma(r_m+1)}{r_k}I''[T] - \Delta V[T] - \frac{\Delta(r_m+1)}{r_k}V''[T] + U''[T] = 0. \quad (29)$$

By assuming the dimensionless harmonic base excitation equals to $U'' = -A_{ex}\sin\Omega T$, the first-order periodic solution of the displacement, voltage, and current are, respectively, defined by:

$$X[T] = a_1\cos[\Omega T] + a_2\sin[\Omega T], \quad (30)$$

$$V[T] = b_1\cos[\Omega T] + b_2\sin[\Omega T], \quad (31)$$

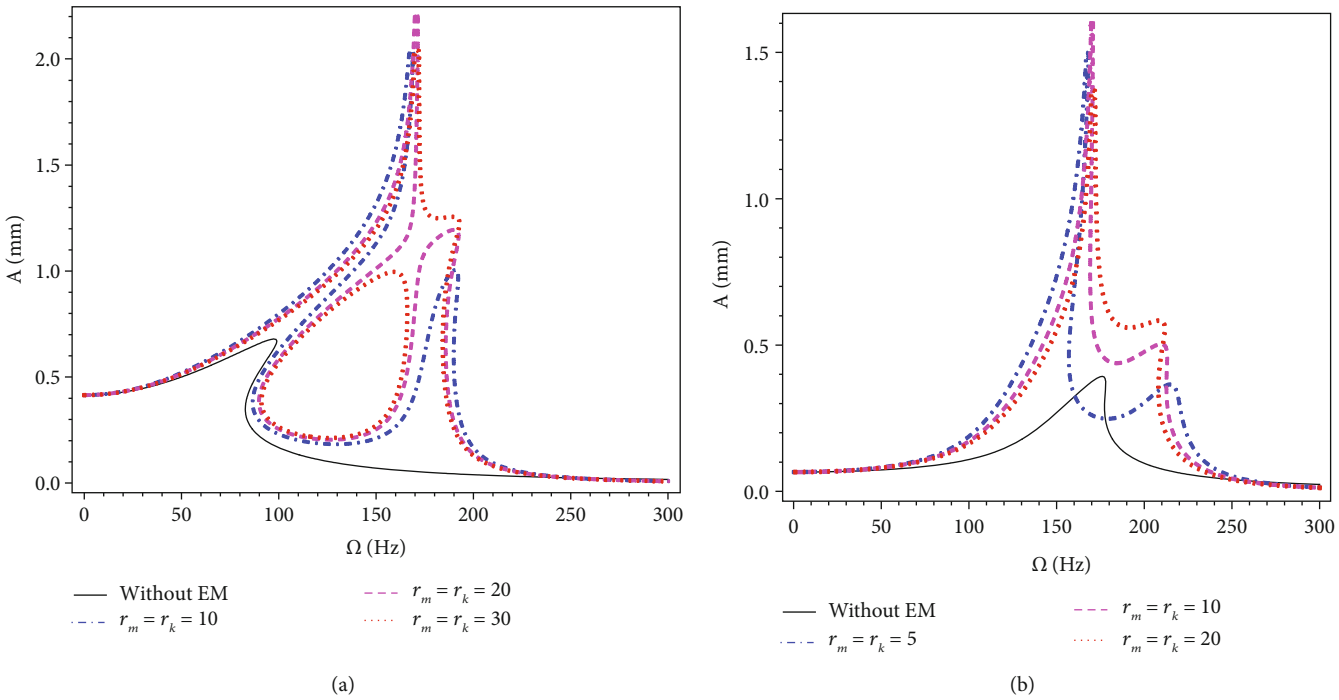

FIGURE 5: Maximum displacements versus excitation frequency of cantilever at different values of mass and stiffness ratios, when $a_{ex} = 2$ g; (a) $d = 7.5$ mm, (b) $d = 6.5$ mm.

$$I[T] = c_1 \cos[\Omega T] + c_2 \sin[\Omega T], \tag{32}$$

$$U[T] = U_b \sin[\Omega T] \longrightarrow U'' = -A_{ex} \sin[\Omega T], \tag{33}$$

in which $\Omega = \omega_{ex}/\omega_e$ is the dimensionless excitation frequency and $A_{ex} = a_{ex}/(l\omega_e{}^2)$ is dimensionless exciting acceleration amplitude. Substituting Equations (30)–(33) into Equations (21) and (29), equaling the coefficients of $\sin \Omega T$ and $\cos \Omega T$, respectively, six equations around variable coefficients a_1, a_2, b_1, b_2, c_1, and c_2 can be obtained as:

$$\left(\Theta_1{}^2 + \Omega^2\right) b_1 + a_2 \Theta_1 \kappa^2 \Omega + a_1 \kappa^2 \Omega^2 = 0, \tag{34}$$

$$\left(\Theta_1{}^2 + \Omega^2\right) b_2 - a_1 \Theta_1 \kappa^2 \Omega + a_2 \kappa^2 \Omega^2 = 0, \tag{35}$$

$$\left(\alpha^2 + \Omega^2\right) c_1 - a_2 \alpha \Theta_2 \Omega + a_1 \Theta_2 \Omega^2 = 0, \tag{36}$$

$$\left(\alpha^2 + \Omega^2\right) c_2 + a_1 \alpha \Theta_2 \Omega - a_2 \Theta_2 \Omega^2 = 0, \tag{37}$$

$$D_2 a_2 + D_1 a_1 + D_3 b_2 + D_4 c_2 = -A_{ex}, \tag{38}$$

$$D_2 a_1 - D_1 a_2 + D_3 b_1 + D_4 c_1 = 0, \tag{39}$$

in which:

$$D_1 = \frac{\left(-2r_k \zeta \Omega + 2\zeta \Omega^3 + 2r_m \zeta \Omega^3\right)}{r_k}, \tag{40}$$

$$D_2 = \frac{\left(-\Omega^2 - r_k \Omega^2 + r_m \Omega^4 - a\left(r_k - r_m \Omega^2\right)\right)}{r_k} + \frac{3A^2 b r_m \Omega^2}{2r_k} + \frac{3A^2 b}{4}, \tag{41}$$

$$D_3 = \frac{\left(-r_k \Delta + \Delta\Omega^2 + r_m \Delta \Omega^2\right)}{r_k}, \tag{42}$$

$$D_4 = \frac{\gamma\left(r_k - (1 + r_m)\Omega^2\right)}{r_k}. \tag{43}$$

Parameter A represents the vibration amplitude of the beam tip, where $A^2 = a_1{}^2 + a_2{}^2$ can be obtained. Substituting Equation (40) into Equation (6), the following equations are obtained:

$$a_2\left(D_2 - D_3 \frac{\kappa^2 \Omega^2}{\Theta_1{}^2 + \Omega^2} + D_4 \frac{\Theta_2 \Omega^2}{\alpha^2 + \Omega^2}\right) + a_1\left(D_1 + D_3 \frac{\Theta_1 \kappa^2 \Omega}{\Theta_1{}^2 + \Omega^2} - D_4 \frac{\alpha \Theta_2 \Omega}{\alpha^2 + \Omega^2}\right) = -A_{ex}, \tag{44}$$

$$a_1\left(D_2 - D_3 \frac{\kappa^2 \Omega^2}{\Theta_1{}^2 + \Omega^2} + D_4 \frac{\Theta_2 \Omega^2}{\alpha^2 + \Omega^2}\right) - a_2\left(D_1 + D_3 \frac{\Theta_1 \kappa^2 \Omega}{\Theta_1{}^2 + \Omega^2} - D_4 \frac{\alpha \Theta_2 \Omega}{\alpha^2 + \Omega^2}\right) = 0. \tag{45}$$

Using Equations (44) and (45), one can obtain the frequency-response equation as:

$$\left(D_2 - D_3 \frac{\kappa^2 \Omega^2}{\Theta_1{}^2 + \Omega^2} + D_4 \frac{\Theta_2 \Omega^2}{\alpha^2 + \Omega^2}\right)^2 A^2 + \left(D_1 + D_3 \frac{\Theta_1 \kappa^2 \Omega}{\Theta_1{}^2 + \Omega^2} - D_4 \frac{\alpha \Theta_2 \Omega}{\alpha^2 + \Omega^2}\right)^2 A^2 = A_{ex}{}^2. \tag{46}$$

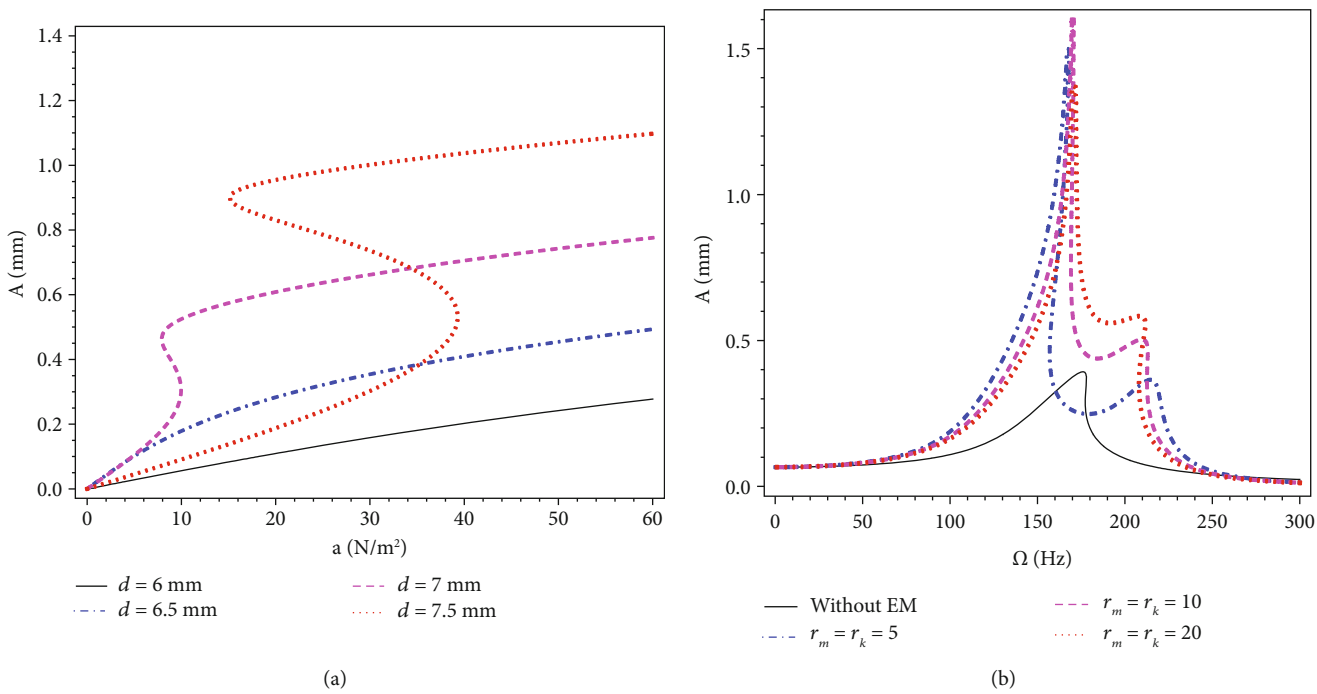

FIGURE 6: Vibration amplitude versus excitation level for (a) different d values and (b) different r_m and r_k.

Substituting Equation (40) into Equation (46), and considering Equation (30) and (34), the current and voltage solutions can be obtained as:

$$V = \sqrt{{b_1}^2 + {b_2}^2} = A\sqrt{\frac{\kappa^2\Omega}{{\Theta_1}^2 + \Omega^2}},$$
$$I = \sqrt{{c_1}^2 + {c_2}^2} = A\sqrt{\frac{\Theta_2\Omega}{\alpha^2 + \Omega^2}}. \quad (47)$$

Therefore, the power of each circuit can be obtained:

$$P_V = \frac{1}{2}\Theta_1 V^2 = \frac{1}{2}\frac{\Theta_1\,\kappa^4\Omega^2}{{\Theta_1}^2 + \Omega^2}A^2,$$
$$P_I = \frac{1}{2}\alpha_1 I^2 = \frac{1}{2}\frac{\alpha_1{\Theta_2}^2\Omega^2}{\alpha^2 + \Omega^2}A^2. \quad (48)$$

6. Numerical Results and Discussion

The geometrical, physical, and mechanical properties of the HEH+DM model, including the piezoelectric and magnetostrictive layers, are itemized in Table 1.

6.1. Validation of Results and Frequency-Response Analysis. Magnetic potential energy is the main factor affecting the nonlinearity of the energy-harvesting system. Adjusting the distance d between the magnets can change the nonlinear properties and strength. The curves of the linear stiffness and nonlinear stiffness of the system as a function of d are given in Figure 2. when $d = d_0 = 7.5$ mm, the linear stiffness $k = 0$, so d_0 is the critical point; when $d < d_0$, $k < 0$, and $k_3 > 0$, the system is a bistable structure; when $d > d_0$: $k > 0$, $k_3 > 0$, the system exhibits a monostable characteristic. At present, the system has bistable appearances.

It can be seen when $d < 7.5$ mm, the system is a bistable structure. The bistable structure is one of the current research hotspots in the field of energy harvesting. The form of motion includes large-amplitude limit cycle oscillation, small-amplitude limit cycle oscillation, burst chaotic motion, and continuous chaotic motion. This paper attempts to analyze this type of system by using the harmonic balance method and discusses the external parameters (level of acceleration, excitation frequency, magnet spacing, etc.) on the system response and output power.

Figure 2(c) represents the nonlinear potential energy versus the free end of the cantilever beam displacement curve at five different parameter d values. As seen in Figure 3, the numerical results of the present study have been verified with experimental results ref. [40] for a cantilever EH with Ms layer, without tip mass, nonlinear magnetic force, and DM. Figure 3 illustrates the comparison of the frequency-responses of the displacement and generated power of results from ref. [40] performances and present study for a traditional cantilever Ms-EH. There is a small relative difference between the present study and experimental results [40], for the tip displacement and harvested power. Also, to verify the preeminence of the HEH mathematical model, this study used a typical MsEH (without the piezoelectric part) for validation. Response curves are demonstrated at Figure 4 with two different stiffness ratio ($r_k = K_0/K_e$) of HEH+DM. The results showed good agreement with the literature (Cao et al. [27]) at various excitation frequencies.

In this subsection, the frequency-response curves are plotted to investigate the effects of various parameters such as r_m and r_k on the harvester responses. In Figure 5(a) the

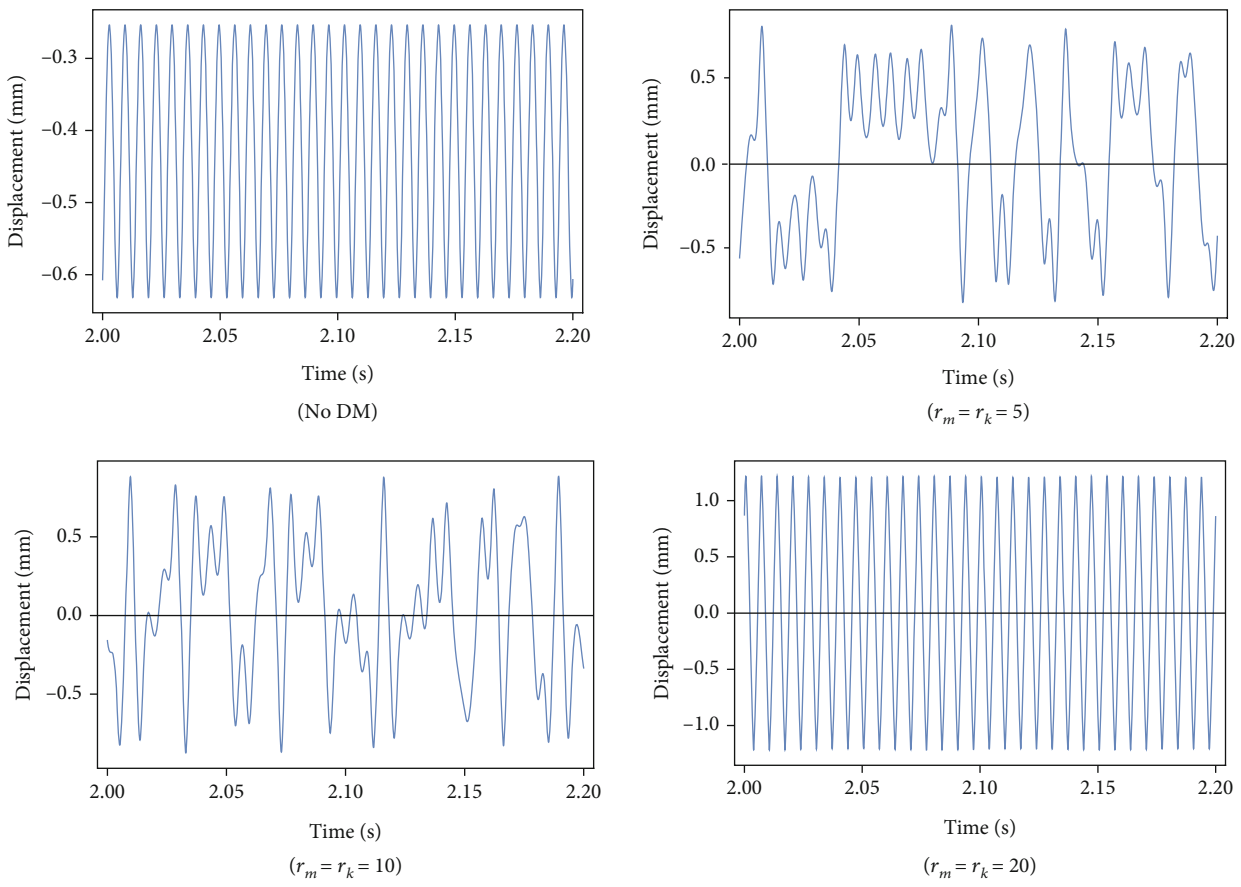

(a)

Figure 7: Continued.

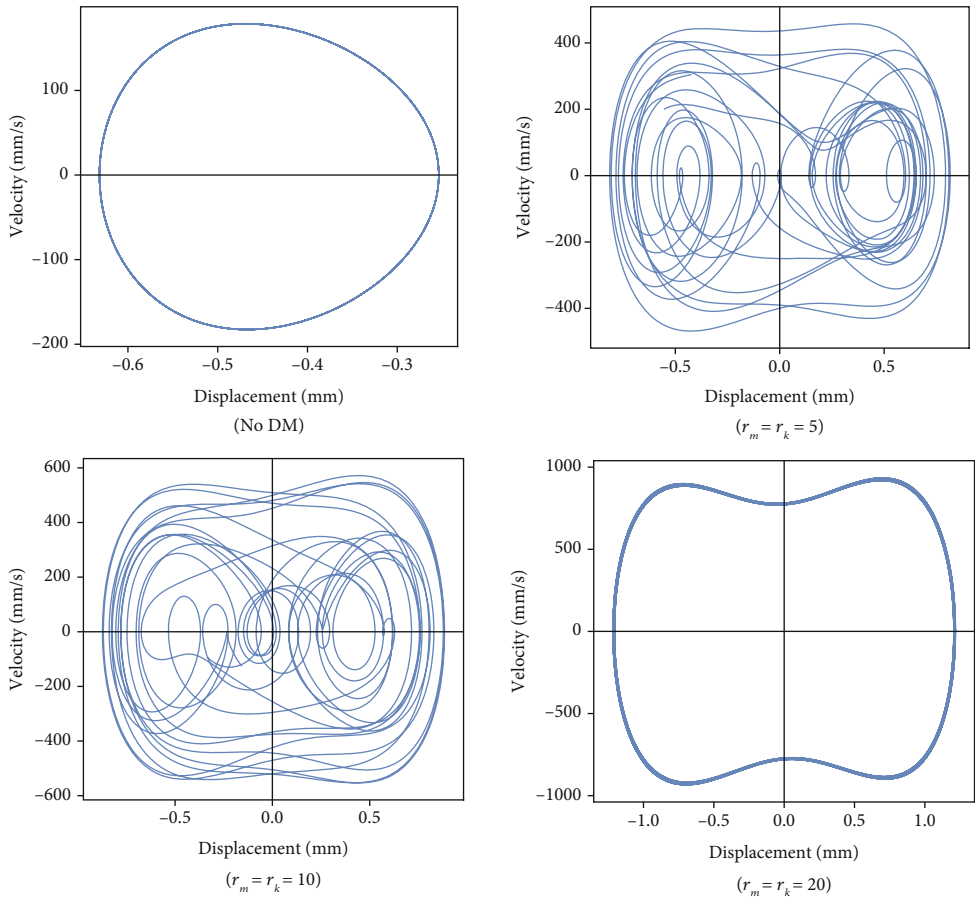

(b)

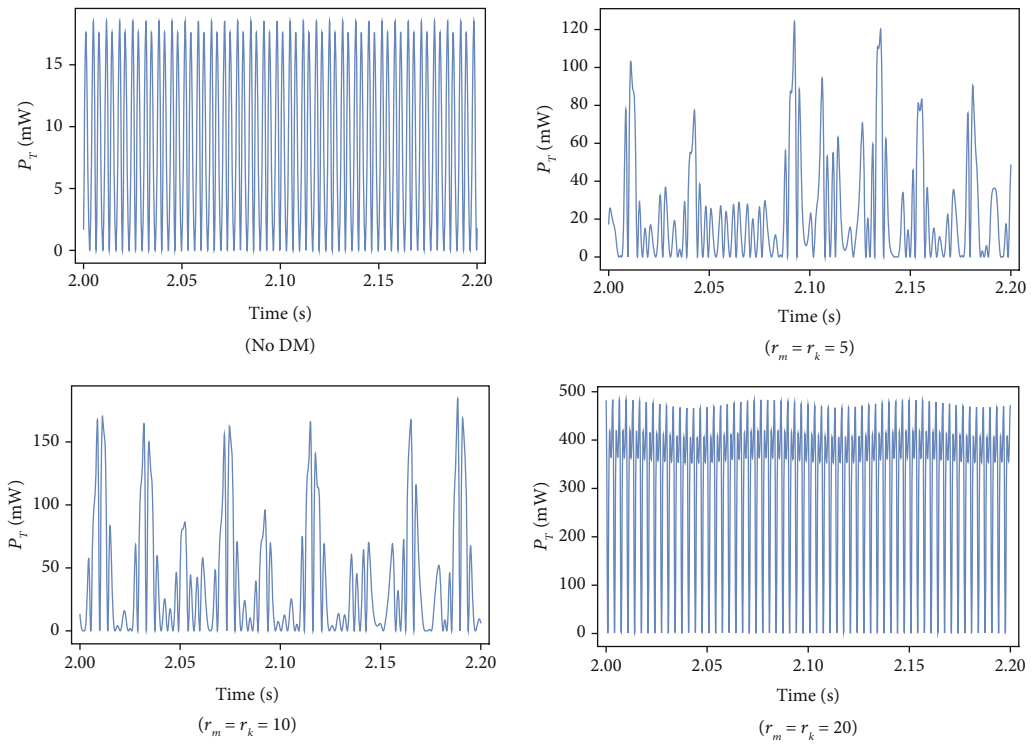

(c)

Figure 7: Continued.

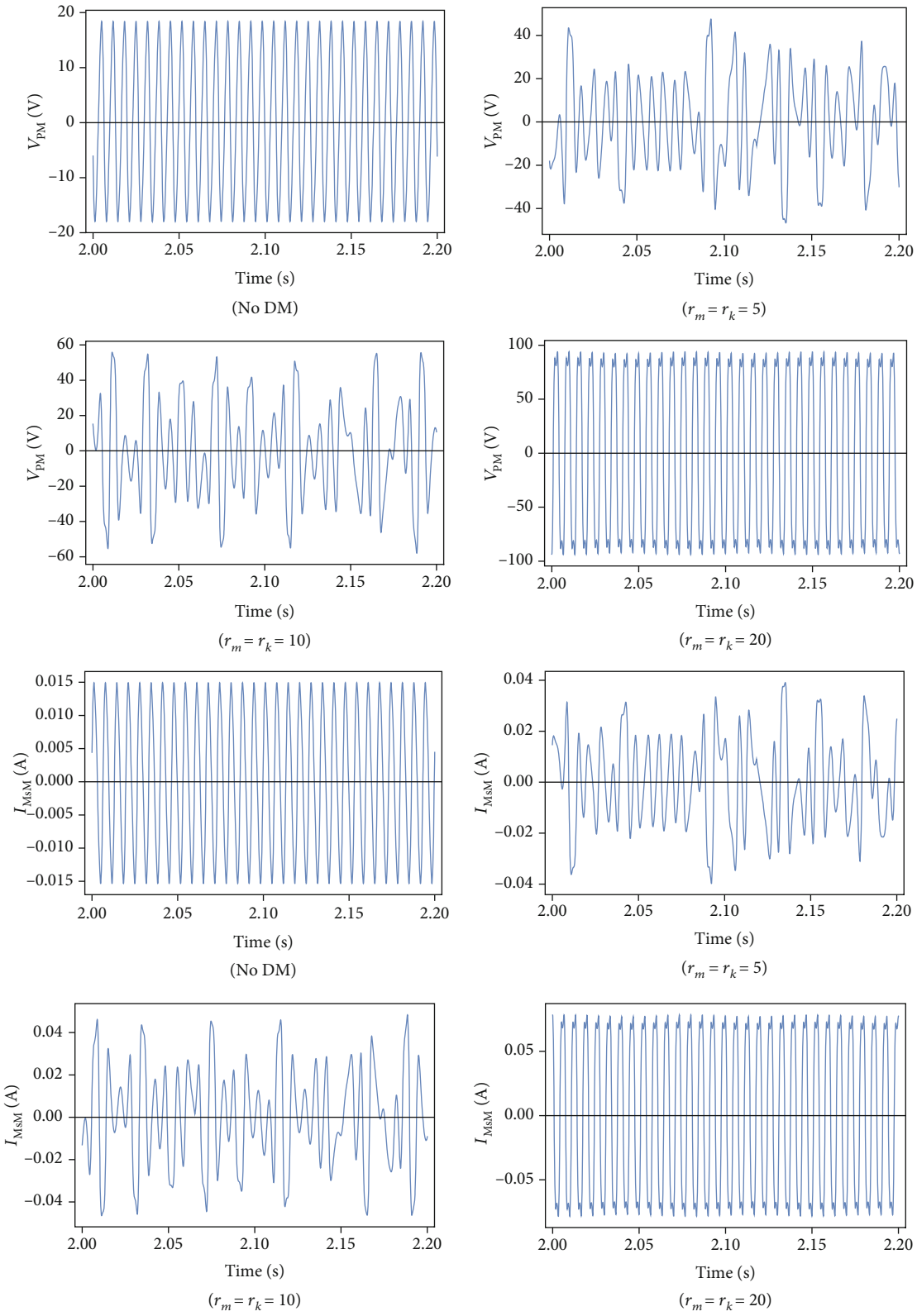

Figure 7: (a) Comparison of the time response of the beam oscillation at different r_m and r_k values. (b) Comparison of the phase portrait diagram of beam tip for different r_m and r_k values. (c) Comparison of the total harvested power of hybrid system at different r_m and r_k values. *d*: time responses of piezoelectric part voltage and Ms part current at different r_m and r_k values.

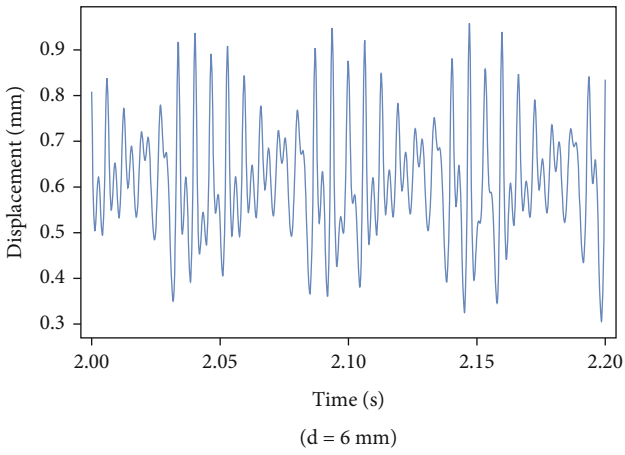

(d = 6 mm)

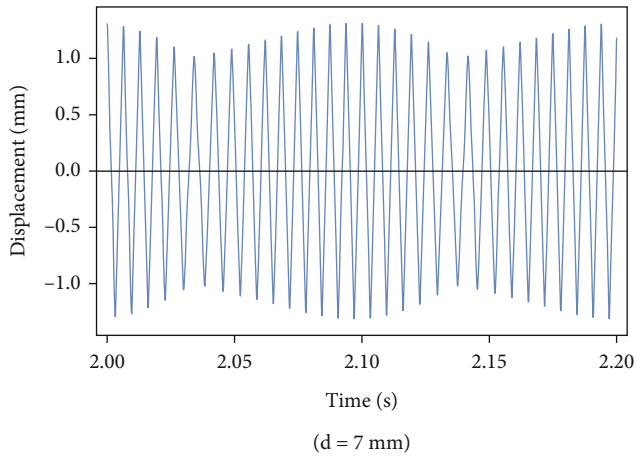

(d = 7 mm)

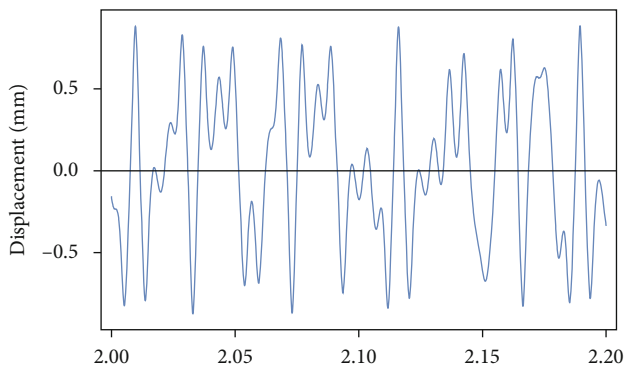

(d = 6.5 mm)

(a)

Figure 8: Continued.

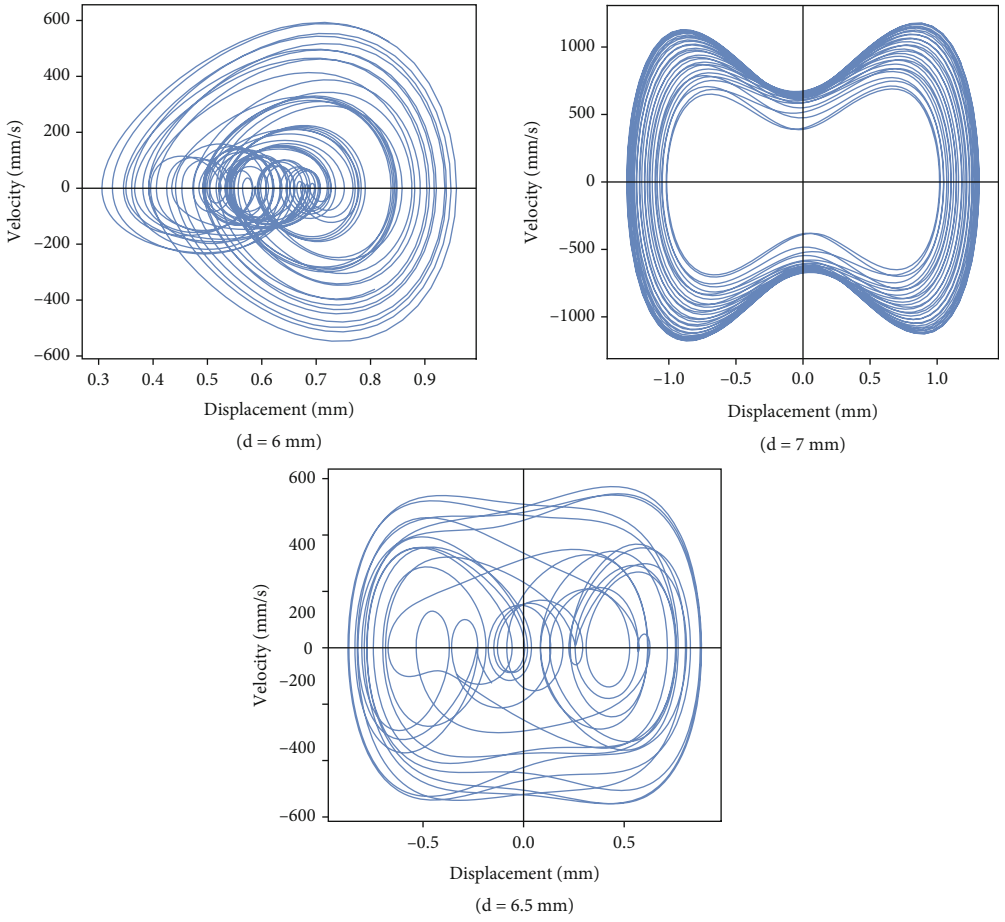

(b)

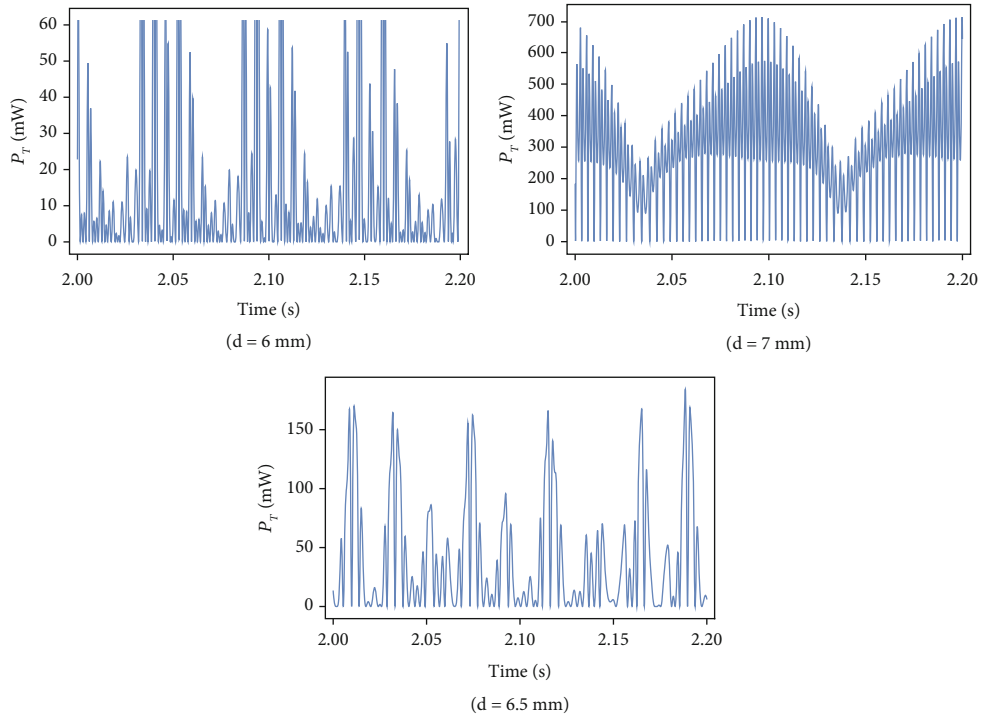

(c)

Figure 8: Continued.

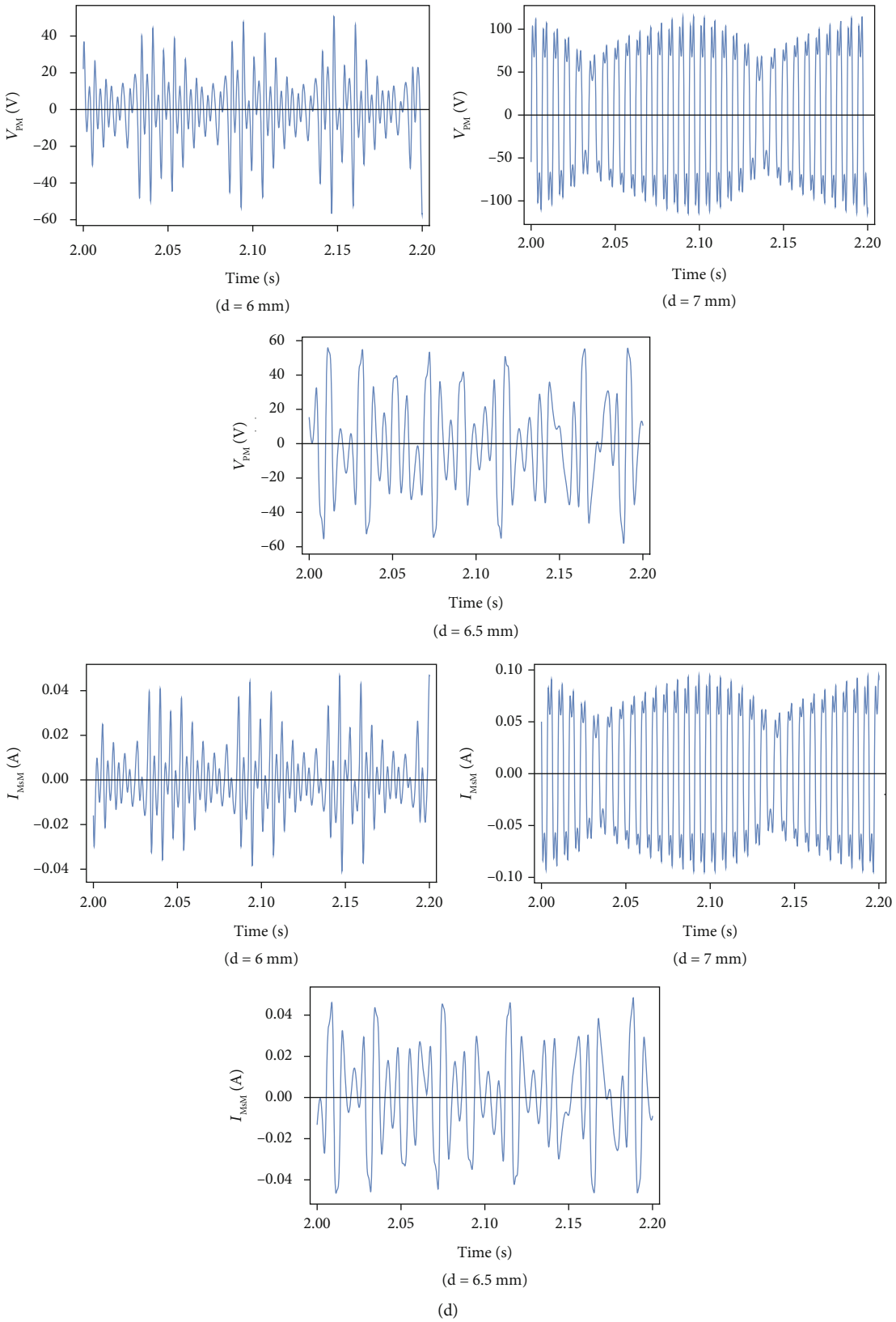

Figure 8: (a) Comparison of the time response of the beam oscillation at different values of parameter d (with $r_m = 10$, $\omega_{ex} = 150$, and $a_{ex} = 2$ g). (b) Comparison of the phase portrait of the beam oscillation at different values of parameter d (with $r_m = 10$, $\omega_{ex} = 150$, and $a_{ex} = 2$ g). (c) Comparison of the output power of the hybrid harvester at different values of parameter d (with $r_m = 10$, $\omega_{ex} = 150$, and $a_{ex} = 2$ g). (d) Time responses of piezoelectric part voltage and Ms part current at different values of parameter d.

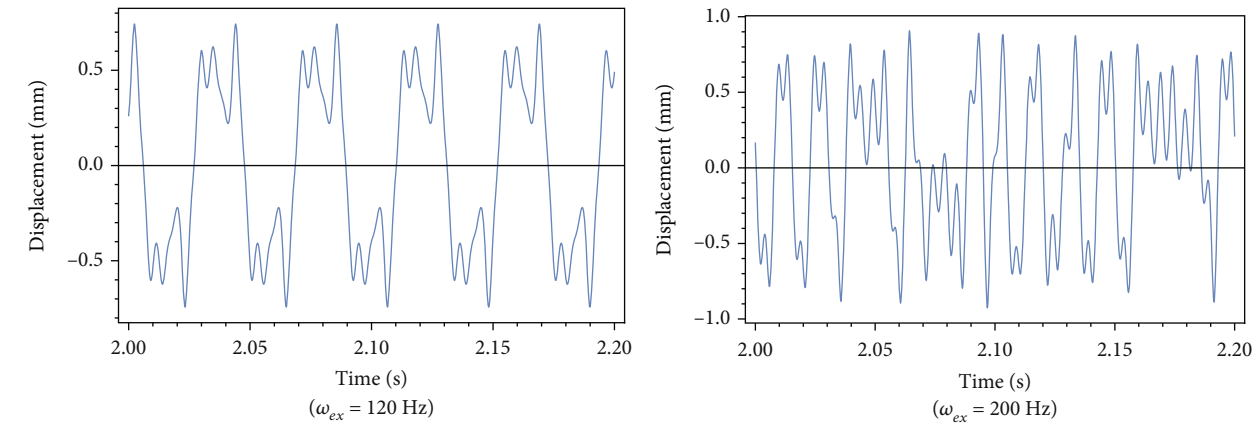

(a)

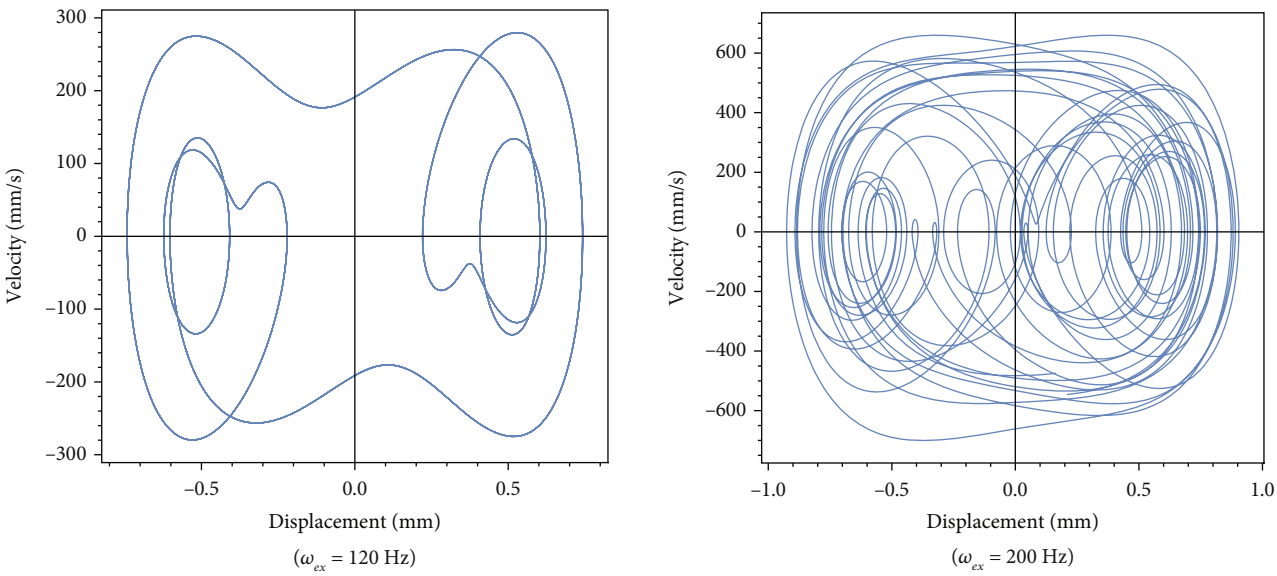

(b)

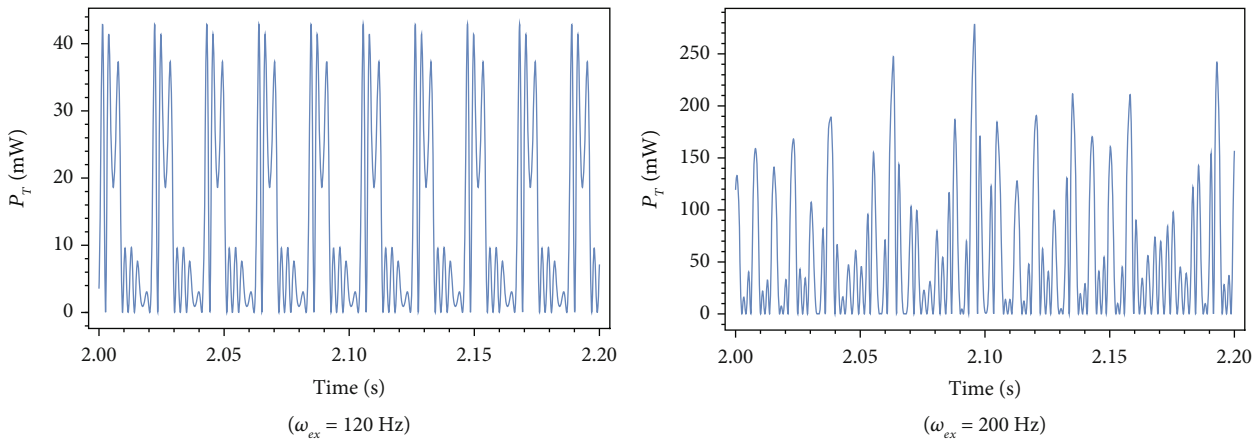

(c)

Figure 9: Continued.

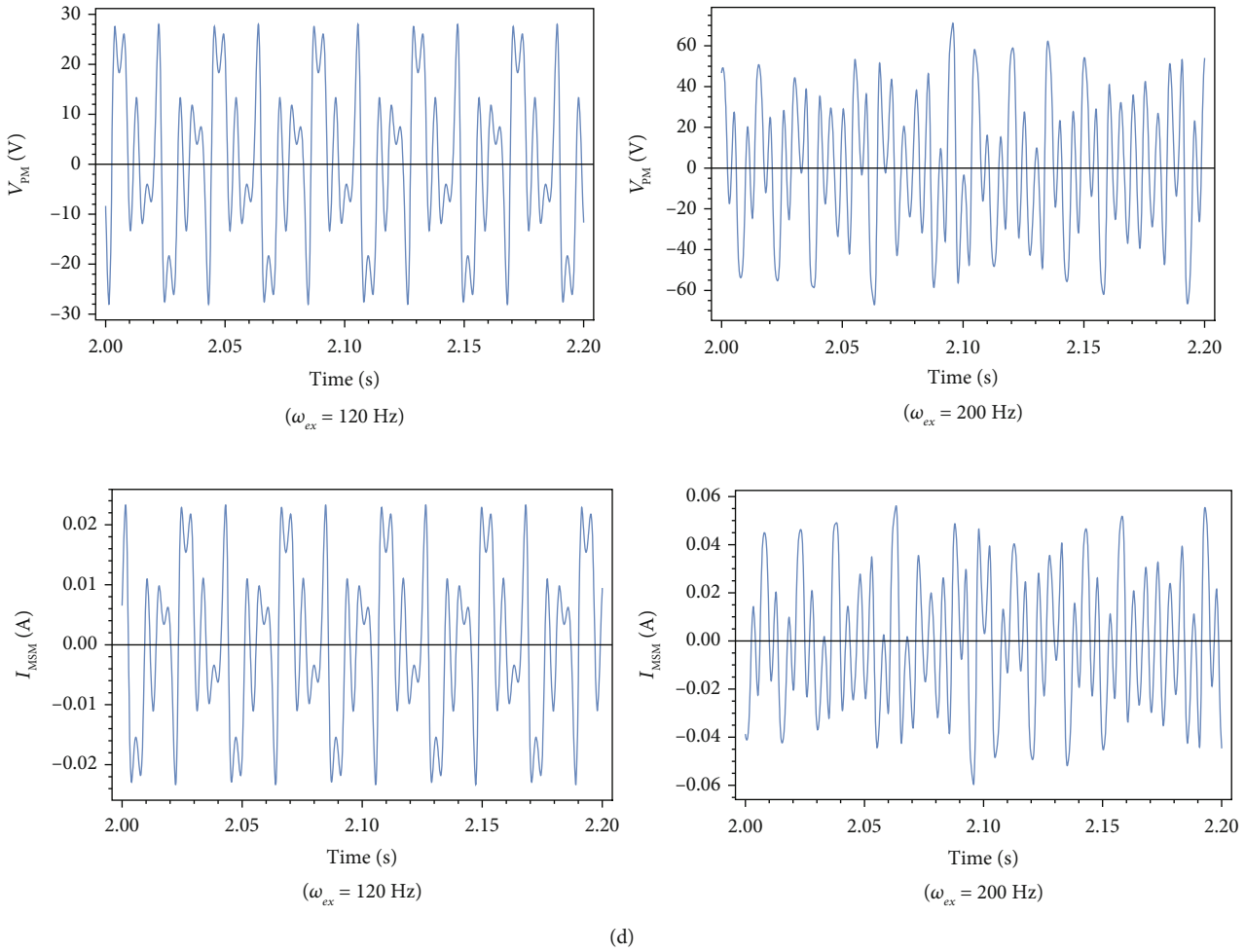

Figure 9: (a) Comparison of the time response of the beam oscillation at two different values of ω_{ex}. (b) Comparison of the phase portrait of the beam oscillation at two different values of ω_{ex}. (c) Comparison of the total power of hybrid harvester at two different values of ω_{ex}. (d) Time responses of piezoelectric part voltage and Ms part current at different values of ω_{ex}.

frequency-response curves are plotted for vibration of tip mass and harvested voltage, respectively, at different values of mass and stiffness ratios. As we can see, there are two resonance peaks in the frequency-response of 2-DOF vibrational systems except in the harvester with no elastic substructure. Also, response curves bend to the right noticeably, because of the nonlinear magnetic force. Without EM, the resonant frequency equals $\omega_{ex} = 100Hz$, and the max of amplitude is equal to $A = 0.68$ mm. Besides, there are three solutions in the frequency domain $80Hz < \omega_{ex} < 100Hz$, also the min and max responses are stable responses, and the middle one is unstable.

As shown in Figure 5(a) when the stiffness and mass ratios equal 10, two resonant frequencies occurred at $\omega_{ex} =$ 170 Hz and $\omega_{ex} = 195$ Hz, and the max vibration amplitudes equal to $A = 2.05$ mm and $a_{ex} = 1$ mm, respectively. Also, there are three solutions for the vibration amplitude when excitation frequency bands are $88 < \Omega < 170$ or $190 < \omega_{ex} <$ 195 in which these two regions have two stable responses. But when $\omega_{ex} < 88$, $\omega_{ex} > 195$, or $170 < \omega_{ex} < 190$, the system has one stable response. It should be noted that frequencies of 88 Hz and 190 Hz are called escape points. When $r_m = r_k = 30$, two frequency peaks occurred at $\omega_{ex} =$170 Hz and $\omega_{ex} =$195 Hz, in which the maximum responses were equal to 2.2 mm and 1.2 mm, respectively; also, the escape points occurred at $\omega_{ex} =$92 Hz and $\omega_{ex} =$185 Hz. The graphs in Figure 5(b) illustrate the influence of the r_m and r_k amplitudes on the response. In the case of vibrations with the amplitude $r_m = r_k = 20$, the highest values of displacement of the beam of the HEH system, $A \geq 0.5$ mm are observed in the range of the frequency variability $\omega_{ex} \in [145,215]$. In relation to the case with $r_m = r_k = 10$ and $r_m = r_k = 5$, this zone is narrower and falls within the variability bond of $\omega_{ex} \in [140,175]$ and $\omega_{ex} \in [130,155]$, respectively. A system with DM more effectively recovers energy in the range of $\omega_{ex} \in [50,250]$. In the case of HEH with $r_m = r_k = 5$, a sharp decrease in the vibration level and the efficiency of energy extraction is observed in the zone $\omega_{ex} \in [166,178]$.

The relations between the vibration amplitude and the excitation level with different distances d are plotted in Figure 6 when $r_m = r_k = 10$ and $\omega_{ex} = 120$ Hz. For the harvester, the escape phenomena looks at a higher excitation level with an increasing d value, for example, this phenomena occurred for $d = 7.5$ mm, when the level is $a_{ex} = 3.8$ g

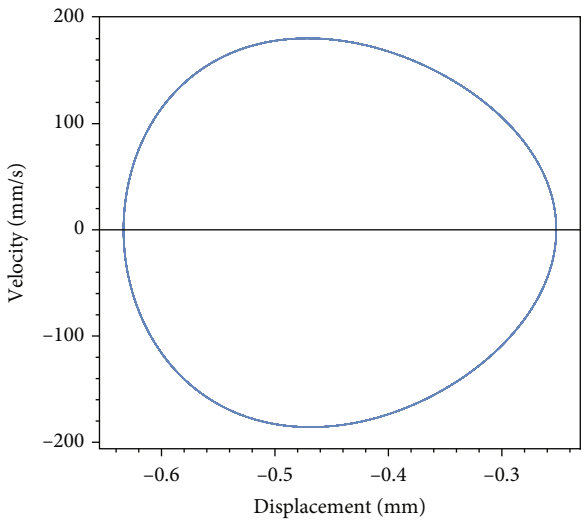

(a_{ex} = g)

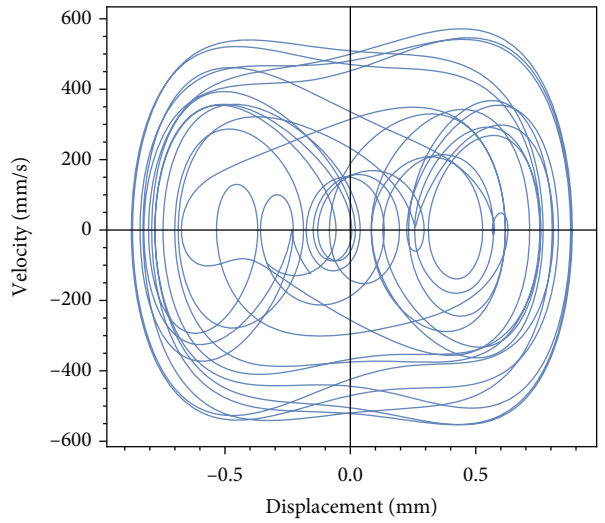

(a_{ex} = 2g)

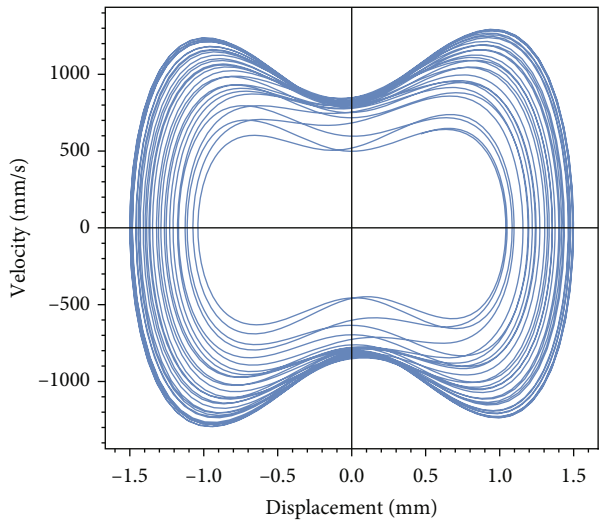

(a_{ex} = 3g)

(a)

Figure 10: Continued.

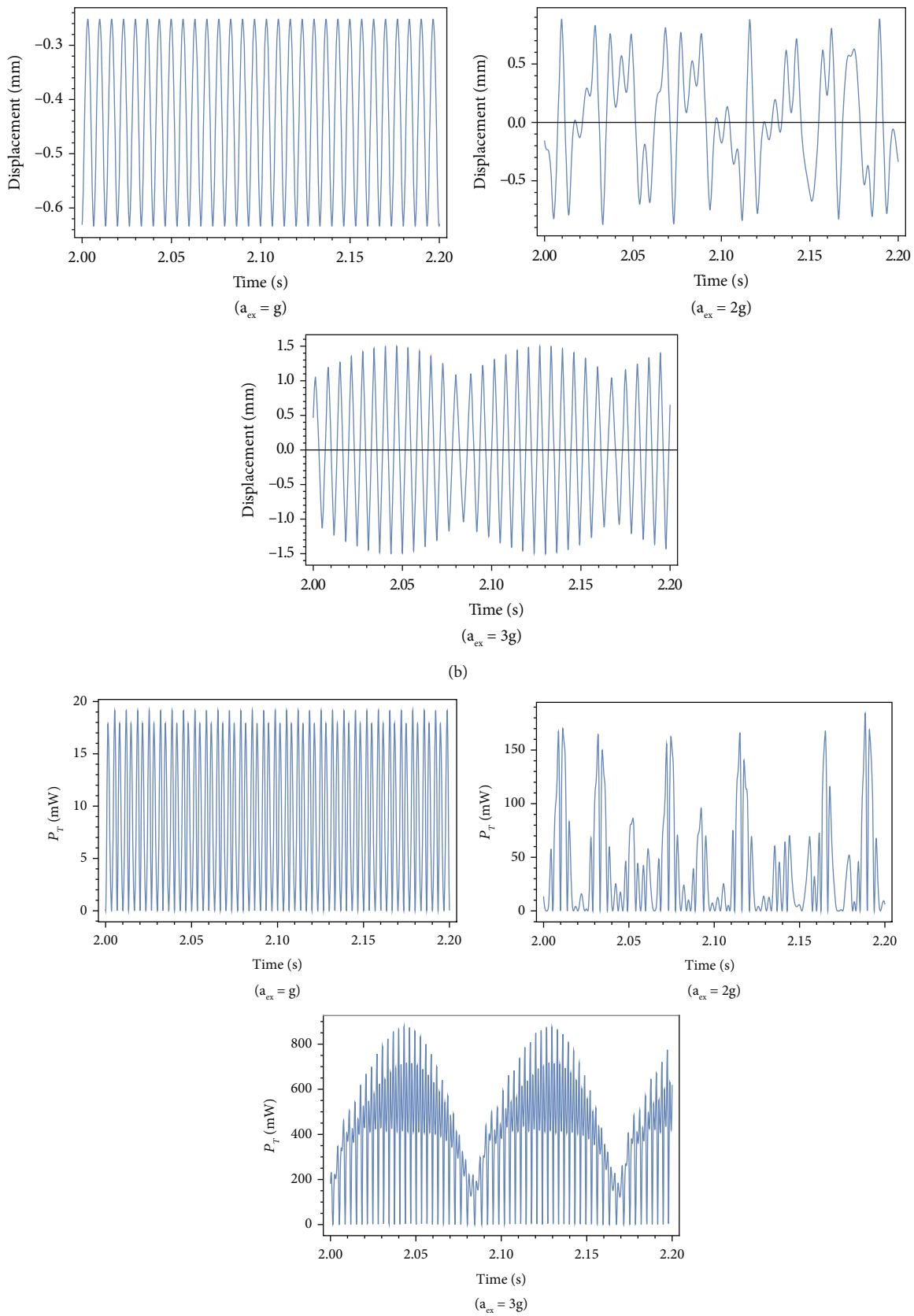

Figure 10: Continued.

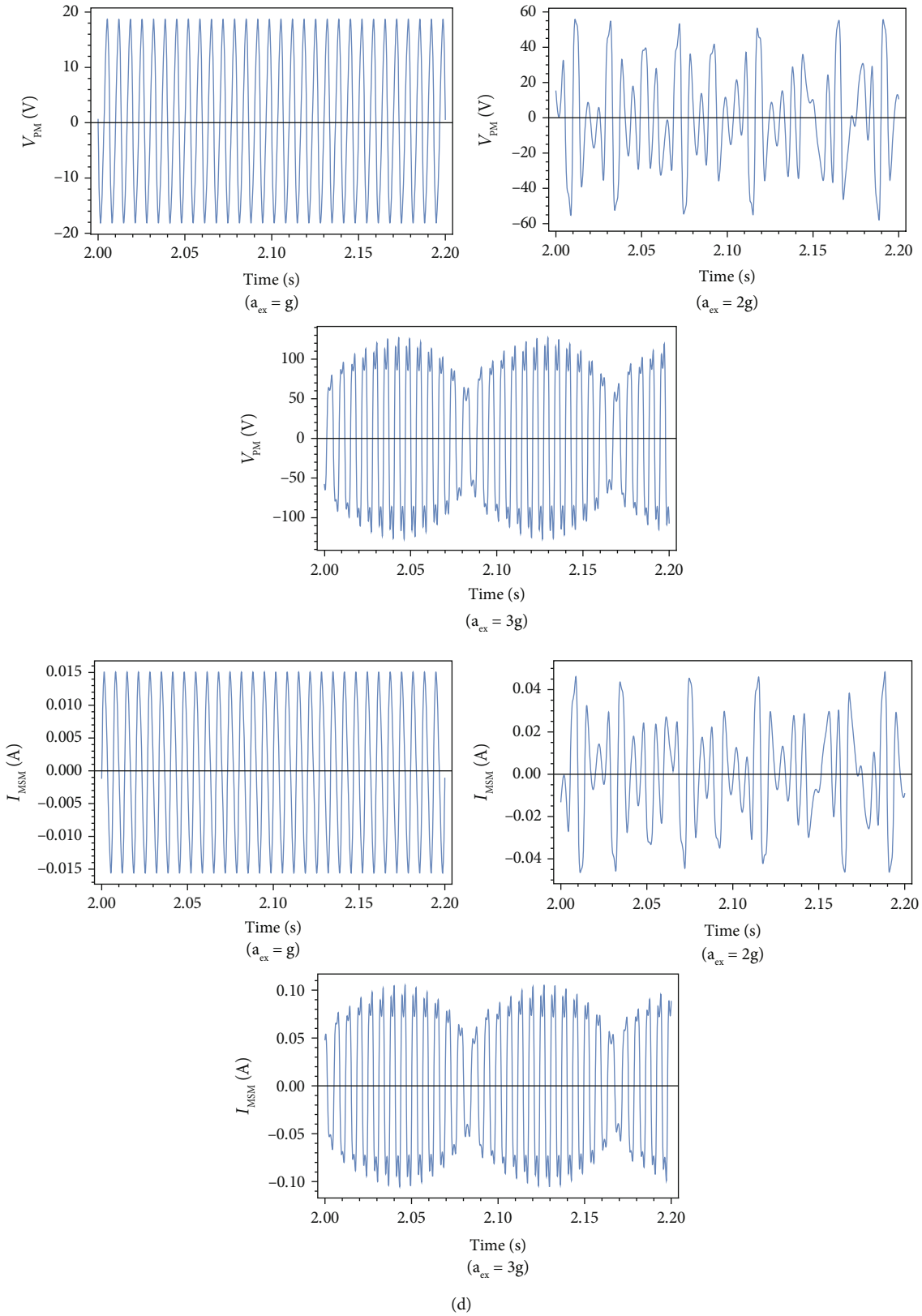

Figure 10: (a) Comparison of the phase portrait of the beam oscillation at different values of a_{ex}. (b) Comparison of the time response of the beam oscillation at different values of a_{ex}. (c) Comparison of the total power of hybrid harvester at two different values of a_{ex}. (d) Time responses of piezoelectric part voltage and Ms part current at different values of a_{ex}.

and for $d = 7$ mm at $a_{ex} = 1.1$ g, correspondingly. The relations between the displacement amplitude and the excitation level with various parameters r_m and r_k are plotted in Figure 5(b), when $d = 7$ mm, $\omega_{ex} = 150$ Hz. For the harvester, the escape phenomena occurred at a minor a_{ex} by decreasing r_m and r_k values, for example, the escape appears at $a_{ex} = 1.5$ g when $r_m = r_k = 20$ and at $a_{ex} = 2.2$ g when $r_m = r_k = 10$, correspondingly. The plots demonstrated that the greater mass and stiffness ratios are advantageous for the HPH +DM to stun the potential barrier and had a high-orbit motion at low excitation levels.

6.2. Time Response Analysis. This article uses the Runge-Kutta method to solve Equation (26) to study the output features of the NHEH. For easiness, the impact of the initial condition in terms of the simultaneous solution is not the subject of analysis in this paper. The vibration response, phase plane diagram of the beam, and total output power of harvester are plotted in Figure 7 for various r_m and r_k amplitudes with $d = 7mm$, $\omega_{ex} = 150Hz$, and $a_{ex} = 2g$.

Without DM, the beam oscillates about an equilibrium point with very small tip velocity and vibrations, causing the intrawell motion and low harvested power. If the mass and stiffness ratios increased, the output power is chaotic because of the motion of the beam tip among two wells. By extra rising, the r_m and r_k values, the beam tip shows a high-energy interwell motion, considered by a periodic oscillation with high amplitude, causing the substantial increase of the vibration amplitudes and the harvested power.

Figures 8(a)–8(d) are plotted the graphs for various d parameters. As demonstrated in Figure 8, when $d = 6mm$, the beam oscillates about an equilibrium point with small tip velocity and vibrations, causing the intrawell motion and low harvested voltage. As shown in Figure 8, if the distance increased, the output voltage is chaotic among the two wells. Considering Figure 8, by increasing instance to $d = 7$ mm, the beam shows a high-energy motion amplitude, and the harvested power increases.

Figures 9(a)–9(d) plot the output voltage and phase portrait diagrams of HEH+DM for different excitation frequencies. As shown in these plots, by increasing the excitation frequencies toward the higher values, in which $\omega_{ex} < 150Hz$, the harvester shows high amplitude bistable motions between the potential wells.

As shown in Figures 10(a)–10(d), the output power and phase diagram of the harvester are plotted at different excitation levels when $d = 7mm$, $\omega_{ex} = 150Hz$, and $r_m = r_k = 10$. With lower excitation levels, there is chaotic motion inside the wells.

7. Conclusion

This paper offers a hypothetical background for the design of high proficiency hybrid vibration energy harvester. The employed principle and the corresponding theoretical model of HEH are explained in detail and established based on the lumped-parameter model, the second law of Newton, and Kirchhoff's law. The 2-DOF model and the frequency-response analytical expressions of the NHEH+DM are derived, and the properties of the harvester are studied. The recognized parameters of the vibration harvester are as declared; then the distance d and r_m and r_k ratios are design constraints to magnify vibration energy. By changing the mass and stiffness ratios at a certain value of d, the harvester can display various dynamic motion forms under different excitation levels, including intrawell periodic low-energy oscillation (small-amplitude motion), interwell chaotic oscillation, and interwell periodic high-energy oscillation (large-amplitude motion). By investigation of the electromechanical coupled model, numerical results showed that the DM could intensely enhance the generating power and broader exciting frequency band.

Data Availability

The data that support the findings of this study are available on request from the corresponding author, kazemzadeh@iaushiraz.ac.ir.

Conflicts of Interest

The authors declare that they have no conflicts of interest.

References

[1] S. P. Beeby, R. N. Torah, M. J. Tudor et al., "A micro electromagnetic generator for vibration energy harvesting," *Journal of Micromechanics and microengineering*, vol. 17, no. 7, pp. 1257–1265, 2007.

[2] H. Liu, W. Li, X. Sun, C. Cong, C. Cao, and Q. Zhao, "Enhanced the capability of magnetostrictive ambient vibration harvester through structural configuration, premagnetization condition and elastic magnifier," *Journal of Sound and Vibration*, vol. 492, p. 115805, 2021.

[3] X. Bai, Y. Wen, P. Li, J. Yang, X. Peng, and X. Yue, "Multimodal vibration energy harvesting utilizing spiral cantilever with magnetic coupling," *Sensors and Actuators A: Physical*, vol. 209, pp. 78–86, 2014.

[4] L. Tang, Y. Yang, and C.-K. Soh, "Improving functionality of vibration energy harvesters using magnets," *Journal of Intelligent Material Systems and Structures*, vol. 23, no. 13, pp. 1433–1449, 2012.

[5] B. Andò, S. Baglio, A. R. Bulsara, V. Marletta, and A. Pistorio, "Investigation of a nonlinear energy harvester," *IEEE Transactions on Instrumentation and Measurement*, vol. 66, no. 5, pp. 1067–1075, 2017.

[6] A. Erturk, J. Hoffmann, and D. J. Inman, "A piezomagnetoelastic structure for broadband vibration energy harvesting," *Applied Physics Letters*, vol. 94, no. 25, article 254102, 2009.

[7] M. Ferrari, V. Ferrari, M. Guizzetti, B. Andò, S. Baglio, and C. Trigona, "Improved energy harvesting from wideband vibrations by nonlinear piezoelectric converters," *Sensors and Actuators A: Physical*, vol. 162, no. 2, pp. 425–431, 2010.

[8] M. A. Karami and D. J. Inman, "Equivalent damping and frequency change for linear and nonlinear hybrid vibrational energy harvesting systems," *Journal of Sound and Vibration*, vol. 330, no. 23, pp. 5583–5597, 2011.

[9] P. Kim and J. Seok, "A multi-stable energy harvester: dynamic modeling and bifurcation analysis," *Journal of Sound and Vibration*, vol. 333, no. 21, pp. 5525–5547, 2014.

[10] D. Pan and F. Dai, "Design and analysis of a broadband vibratory energy harvester using bi-stable piezoelectric composite laminate," *Energy Conversion and Management*, vol. 169, pp. 149–160, 2018.

[11] J. Jiang, S. Liu, D. Zhao, and L. Feng, "Broadband power generation of piezoelectric vibration energy harvester with magnetic coupling," *Journal of Intelligent Material Systems and Structures*, vol. 30, no. 15, pp. 2272–2282, 2019.

[12] M. S. Nguyen, Y.-J. Yoon, and P. Kim, "Enhanced broadband performance of magnetically coupled 2-DOF bistable energy harvester with secondary intrawell resonances," *International Journal of Precision Engineering and Manufacturing-Green Technology*, vol. 6, no. 3, pp. 521–530, 2019.

[13] L. Wang, R. Chen, L. Ren, H. Xia, and Y. Zhang, "Design and experimental study of a bistable magnetoelectric vibration energy harvester with nonlinear magnetic force scavenging structure," *International Journal of Applied Electromagnetics and Mechanics*, vol. 60, no. 4, pp. 489–502, 2019.

[14] A. Kianpoor and K. Jahani, "Modeling and analyzing of energy harvesting from trapezoidal piezoelectric beams," *Iranian Journal of Science and Technology, Transactions of Mechanical Engineering*, vol. 43, no. S1, pp. 259–266, 2019.

[15] M. Heshmati and Y. Amini, "An electromechanical finite element model for new CNTs-reinforced harvesters subjected to harmonic and random base excitations," *ranian Journal of Science and Technology, Transactions of Mechanical Engineering*, vol. 44, no. 1, pp. 163–181, 2020.

[16] Z. Wu and Q. Xu, "Design of a structure-based bistable piezoelectric energy harvester for scavenging vibration energy in gravity direction," *Mechanical Systems and Signal Processing*, vol. 162, p. 108043, 2022.

[17] A. Aladwani, M. Arafa, O. Aldraihem, and A. Baz, "Cantilevered piezoelectric energy harvester with a dynamic magnifier," *Journal of Vibration and Acoustics*, vol. 134, no. 3, p. 31004, 2012.

[18] D. Vasic and F. Costa, "Modeling of piezoelectric energy harvester with multi-mode dynamic magnifier with matrix representation," *International Journal of Applied Electromagnetics and Mechanics*, vol. 43, no. 3, pp. 237–255, 2013.

[19] G.-Q. Wang and W.-H. Liao, "A bistable piezoelectric oscillator with an elastic magnifier for energy harvesting enhancement," *Journal of Intelligent Material Systems and Structures*, vol. 28, no. 3, pp. 392–407, 2016.

[20] G. Wang, W.-H. Liao, B. Yang, X. Wang, W. Xu, and X. Li, "Dynamic and energetic characteristics of a bistable piezoelectric vibration energy harvester with an elastic magnifier," *Mechanical Systems and Signal Processing*, vol. 105, pp. 427–446, 2018.

[21] B. P. Bernard and B. P. Mann, "Increasing viability of nonlinear energy harvesters by adding an excited dynamic magnifier," *Journal of Intelligent Material Systems and Structures*, vol. 29, no. 6, pp. 1196–1205, 2018.

[22] H. Liu, C. Cong, C. Cao, and Q. Zhao, "Analysis of the key factors affecting the capability and optimization for magnetostrictive iron-gallium alloy ambient vibration harvesters," *Sensors*, vol. 20, no. 2, p. 401, 2020.

[23] T. Ueno and S. Yamada, "Performance of energy harvester using iron–gallium alloy in free vibration," *IEEE Transactions on Magnetics*, vol. 47, no. 10, pp. 2407–2409, 2011.

[24] S. Kita, T. Ueno, and S. Yamada, "Improvement of force factor of magnetostrictive vibration power generator for high efficiency," *Journal of Applied Physics*, vol. 117, no. 17, p. 17B508, 2015.

[25] Z.-W. Fang, Y.-W. Zhang, X. Li, H. Ding, and L.-Q. Chen, "Complexification-averaging analysis on a giant magnetostrictive harvester integrated with a nonlinear energy sink," *Journal of Vibration and Acoustics*, vol. 140, no. 2, 2018.

[26] U. Ahmed, J. Jeronen, M. Zucca, S. Palumbo, and P. Rasilo, "Finite element analysis of magnetostrictive energy harvesting concept device utilizing thermodynamic magneto-mechanical model," *Journal of Magnetism and Magnetic Materials*, vol. 486, p. 165275, 2019.

[27] S. Cao, L. Liu, J. Zheng, R. Pan, and G. Song, "Modeling and analysis of Galfenol nonlinear cantilever harvester with elastic magnifier," *IEEE Transactions on Magnetics*, vol. 55, no. 6, pp. 1–5, 2019.

[28] Y.-W. Zhang, C.-Q. Gao, Z. Zhang, and J. Zang, "Dynamic analysis of vibration reduction and energy harvesting using a composite cantilever beam with Galfenol and a nonlinear energy sink," *International Journal of Applied Mechanics*, vol. 13, no. 8, p. 2150089, 2021.

[29] C. S. Clemente, D. Davino, and V. P. Loschiavo, "Analysis of a magnetostrictive harvester with a fully coupled nonlinear FEM modeling," *IEEE Transactions on Magnetics*, vol. 57, no. 6, pp. 1–4, 2021.

[30] H. Liu, L. Zhao, Y. Chang, and C. Cong, "Design and characteristic analysis of magnetostrictive bistable vibration harvester with displacement amplification mechanism," *Energy Conversion and Management*, vol. 243, p. 114361, 2021.

[31] H. Wang, L. Tang, Y. Guo, X. Shan, and T. Xie, "A 2DOF hybrid energy harvester based on combined piezoelectric and electromagnetic conversion mechanisms," *Journal of Zhejiang University SCIENCE A*, vol. 15, no. 9, pp. 711–722, 2014.

[32] G. G. Sengha, W. F. Kenfack, M. S. Siewe, C. B. Tabi, and T. C. Kofané, "Dynamics of a non-smooth type hybrid energy harvester with nonlinear magnetic coupling," *Communications in Nonlinear Science and Numerical Simulation*, vol. 90, p. 105364, 2020.

[33] H. Jahanshahi, D. Chen, Y.-M. Chu, J. F. Gómez-Aguilar, and A. A. Aly, "Enhancement of the performance of nonlinear vibration energy harvesters by exploiting secondary resonances in multi-frequency excitations," *The European Physical Journal Plus*, vol. 136, no. 3, pp. 1–22, 2021.

[34] S. Fang, J. Xing, K. Chen, X. Fu, S. Zhou, and W.-H. Liao, "Hybridizing piezoelectric and electromagnetic mechanisms with dynamic bistability for enhancing low-frequency rotational energy harvesting," *Applied Physics Letters*, vol. 119, no. 24, article 243903, 2021.

[35] X. Li, Z. Li, B. Liu, J. Zhang, and W. Zhu, "Numerical research on a vortex shedding induced piezoelectric-electromagnetic energy harvester," *Journal of Intelligent Material Systems and Structures*, vol. 33, no. 1, pp. 105–120, 2022.

[36] A. Erturk and D. J. Inman, "On mechanical modeling of cantilevered piezoelectric vibration energy harvesters," *Journal of Intelligent Material Systems and Structures*, vol. 19, no. 11, pp. 1311–1325, 2008.

[37] S. Cao, S. Sun, J. Zheng et al., "Modeling and analysis of Galfenol cantilever vibration energy harvester with nonlinear magnetic force," *AIP Advances*, vol. 8, no. 5, p. 56718, 2018.

[38] S. Cao, J. Zheng, Y. Guo et al., "Dynamic characteristics of Galfenol cantilever energy harvester," *IEEE Transactions on Magnetics*, vol. 51, no. 3, pp. 1–4, 2015.

[39] S. Shu, "Dynamic modeling and analysis of a bistable piezoelectric cantilever power generation system," *Acta Physica Sinica*, vol. 61, no. 21, pp. 1–12, 2012.

[40] J.-H. Yoo and A. B. Flatau, "A bending-mode galfenol electric power harvester," *Journal of Intelligent Material Systems and Structures*, vol. 23, no. 6, pp. 647–654, 2012.